# Glaciers determine the sensitivity of hydrological processes to perturbed climate in a large mountainous basin on the Tibetan Plateau

**Yi Nan [1], Fuqiang Tian [1]**

**Affiliation:**

1. State Key Laboratory of Hydroscience and Engineering & Department of Hydraulic Engineering, Tsinghua University, Beijing 100084, China

***Corresponding to*:** Fuqiang Tian

Email: tianfq@tsinghua.edu.cn

## Abstract

The major rivers on the Tibetan Plateau supply important freshwater resources to riparian regions, but are undergoing significant climate change in recent decades. Understanding the sensitivities of hydrological processes to climate change is important for water resource management, but large divergences exist in previous studies because of the uncertainties of hydrological models and climate projection data. Meanwhile, the spatial pattern of local hydrological sensitivities was poorly explored despite the strong heterogeneity on the Tibetan Plateau. This study adopted the climate perturbation method to analyze the hydrological sensitivities of a typical large mountainous basin (Yarlung Tsangpo River, YTR) to climate change. We utilized the tracer-aided hydrological model Tsinghua Representative Elementary Watershed-Tracer-aided version (THREW-T) to simulate the hydrological and cryospheric processes in the YTR basin. Multiple datasets and internal stations were used to validate the model, to provide confidence to the baseline simulation and the sensitivity analysis. Results indicated that: (1) The THREW-T model performed well on simulating the streamflow, snow cover area (SCA), glacier mass balance (GMB), and stream water isotope, ensuring good representation of the key cryospheric processes and a reasonable estimation of runoff components. The model performed acceptably on simulating the streamflow at eight internal stations located in the mainstream and two major tributaries, indicating that the spatial pattern

of hydrological processes was reflected by the model. (2) Increasing temperature led to decreasing annual runoff, smaller inter-annual variation, more even intra-annual distribution, and an earlier maximum runoff. It also influenced the runoff regime by increasing the contributions of rainfall and glacier melt overland runoff, but decreasing the subsurface runoff and snowmelt overland runoff. Increasing precipitation had the opposite effect to increasing temperature. (3) The local runoff change in response to increasing temperature varied significantly, with changing rate of -18.6% to 54.3% for 5℃ of warming. The glacier area ratio (GAR) was the dominant factor of the spatial pattern of hydrological sensitivities to both perturbed temperature and precipitation. Some regions had a non-monotonic runoff change rate in response to climate perturbation, which represented the most dynamic regions within the basin, as they kept shifting between energy and water limited stages. The GAR and mean annual precipitation (MAP) of the non-monotonic regions had a linear relation, and formed the boundary of regions with different runoff trends in the GAR-MAP plot.

## 1. Introduction

The Tibetan Plateau (TP), known as the "Asian Water Tower", is the source region of several major rivers in Asia (e.g., Yarlung Tsangpo-Brahmaputra Lantsang-Mekong, Indus, Ganges). The contributions of runoff in the source regions of TP rivers to the total runoff in whole basins range from 6%-60% (Tang et al., 2019; Wang et al., 2020; Cao and Pan, 2014), sustaining the ecosystems and supplying valuable freshwater resources for downstream livelihoods (Immerzeel et al., 2010; Lutz et al., 2014). The sustainable socioeconomic development and the decision-making of water resource management in the riparian countries around the TP rely heavily on the runoff in the major river basins (Cui et al., 2023). Meanwhile, the TP is a typical high mountainous cryosphere, characterized by large stores of frozen soil and frequent multiphase water transferring, resulting in complex hydrological processes and multiple water sources including rainfall, snowmelt and glacier melt (Li et al., 2019; Yao et al., 2022). The melting processes of frozen water are determined by energy budget, and the runoff change on the TP is extremely sensitive to climate change (Gao et al., 2019). Consequently, understanding hydrological processes and estimating the runoff change on the TP is not only of great practical significance, but also a frontier scientific question in global change.

The TP is undergoing significant climate change in recent decades, with a warming rate twice the global average level (Yao, 2019). Based on the recently released Coupled Model Intercomparison Project Phase 6 (CMIP6) (Eyring et al., 2016), the warming levels of 1.5℃, 2℃ and 3℃ over the TP will be attained around the 2030s, 2050s and 2070s, respectively, and the precipitation is also likely to increase significantly (Cui et al., 2023). The hydrological cycling and water resources will change correspondingly; thus it is important to understand the hydrological processes on the TP and the hydrological response to climate change. Plenty of studies have adopted hydrological models to project the runoff change on the TP in the future, but the reported trends and changing rates varied considerably in existing studies. Wang et al. (2021) and Lutz et al. (2014) projected an increasing runoff trend till the end of 21$^{st}$ century, while Cui et al. (2023) predicted the runoff to decrease before the 2030s and turn over to an increasing trend after that. A primary reason for the divergence in existing studies is the model uncertainties. The parameters are usually inadequately constrained solely by the streamflow observation data because of the complex hydrological processes, resulting in large uncertainties

in the estimation on the contributions of runoff components (Tian et al., 2020; Nan et al., 2021a), which influence the runoff projection significantly. For instance, Lutz et al. (2014) estimated the contribution of glacier melt to annual runoff as 0.86~40.59% in the major TP rivers, resulting in an increasing runoff with climate warming, while Cui et al. (2023) estimated the contribution as 0.73~14.33% and resulting in a decreasing trend in the near future. Nonetheless, recently developed hydrological models integrating key cryospheric processes (e.g., Cui et al., 2023) have been proved as effective tools for hydrological simulations on the TP, and the high-quality datasets of snow and glacier (e.g., Chen et al., 2018; Hugonnet et al., 2022) can provide adequate validation for the corresponding models. Moreover, tracer-aided hydrological models integrating modules of tracer storage, mixture, and transportation processes forced by the outputs of isotopic general circulation models (iGCMs) have proved to constrain the hydrological model uncertainties significantly (He et al., 2019; Birkel and Soulsby, 2015; Stadnyk and Holmes, 2023), especially for the separation of runoff components (Nan et al., 2021a, 2023). These developments of models and datasets bear the potential to provide a more reasonable baseline for streamflow projection.

Another major source of runoff projection uncertainty is the uncertainty of climatic forcing data (Li et al., 2014). The climatic data in the future are generally generated by the general circulation models (GCMs), which cannot be directly adopted in the catchment scale because of the insufficient spatial resolution and accuracy, so downscaling and bias correction are necessary steps in using GCM data at regional scale (Xu et al., 2019; Olsson et al., 2015). However, even being corrected by the observation data during the historical period, the divergence among the outputs of different GCMs is still significant. For example, the difference in the precipitation change over the TP among 22 CMIP6 products could be larger than 50% (Cui et al., 2023). Bloschl and Montanari (2010) pointed out the large uncertainties of studies analyzing the impact of climate change, and compared them to throwing a dice. As an alternative method, producing hypothesized climate change scenarios by perturbing the current temperature and precipitation data has proved to be valuable in investigating the hydrological sensitivities to climate change (Ayguen et al., 2020; Rasouli et al., 2015; He et al., 2021b). The range of climate perturbation is assumed based on the possible change range projected by an ensemble of GCMs, providing a possible runoff change range accordingly (Su et al., 2023; He

et al., 2021b). The climate perturbation method also allows for a deeper analysis of the separate effect of each climatic factor and the compensation effects among them (He and Pomeroy, 2023).

Although plenty of studies have been conducted for the TP rivers to project the runoff change or analyze the hydrological sensitivities to climate change, most of them were conducted at the regional or basin scale (e.g., Su et al., 2023; Zhang et al., 2022b). The local hydrological response to climate change could significantly differ among small catchments due to the different geographical and meteorological characteristics (Bai et al., 2023), which is important for local water resources utilization and management (Zhang et al., 2015). Considering the strong heterogeneity in meteorological factors and land surface conditions in the large river basins on the TP (Wang et al., 2021; Li et al., 2020), the local hydrological sensitivities to climate change should have strong variability over the TP. However, the spatial pattern and influence factors of the local hydrological sensitivities within the basin are poorly explored, partly due to the scarce hydrological stations for model validation, resulting in a lack of confidence in the spatial representation of hydrological processes.

Motivated by the mentioned background, this study utilized the spatially distributed tracer-aided hydrological model THREW-T developed by Nan et al. (2021b) in the Yarlung Tsangpo River basin, a typical large mountainous basin on the Tibetan Plateau, to explore its hydrological sensitivity to perturbed temperature and precipitation. Snow, glacier, isotope data and observation streamflow at nine stations were collected to validate the model. The spatial pattern of the local hydrological sensitivities and the influence factors were analyzed in particular. The main objectives of this study are as follows: (1) to test the performance of THREW-T model on simulating all the hydrological and cryospheric processes in the Yarlung Tsangpo River basin, (2) to analyze the sensitivities of hydrological processes in the Yarlung Tsangpo River basin to a reasonable range of perturbed temperature and precipitation, and (3) to analyze the spatial pattern and the influence factors of the local hydrological sensitivities.

## 2. Data and methodology

### 2.1 Study area

This study focused on the Yarlung Tsangpo River (YTR) basin, the upstream part of the

Brahmaputra River basin, located in the southern TP (Figure 1). The YTR is one of the longest rivers originating from the TP (longer than 2000 km), extending in the range of 27~32°N and 82~97°E with an elevation extent of 2900~6900 m a.s.l. (above sea level). The mean annual precipitation and temperature in the YTR basin are around 500 mm and -0.2 °C, respectively. The YTR has four major tributaries, i.e., DoxungZangbo, Nianchu River, Lhasa River, and Nyang River, from upstream to downstream. The precipitation is dominated by the South Asian monsoon in the Indian Ocean hydrosphere-atmosphere system, resulting in an obviously wet season from June to September. The outlet hydrological station along the mainstream is the Nuxia station, above which the drainage area is approximately $2\times10^5$ km$^2$, and around 1.5% is covered by glaciers.

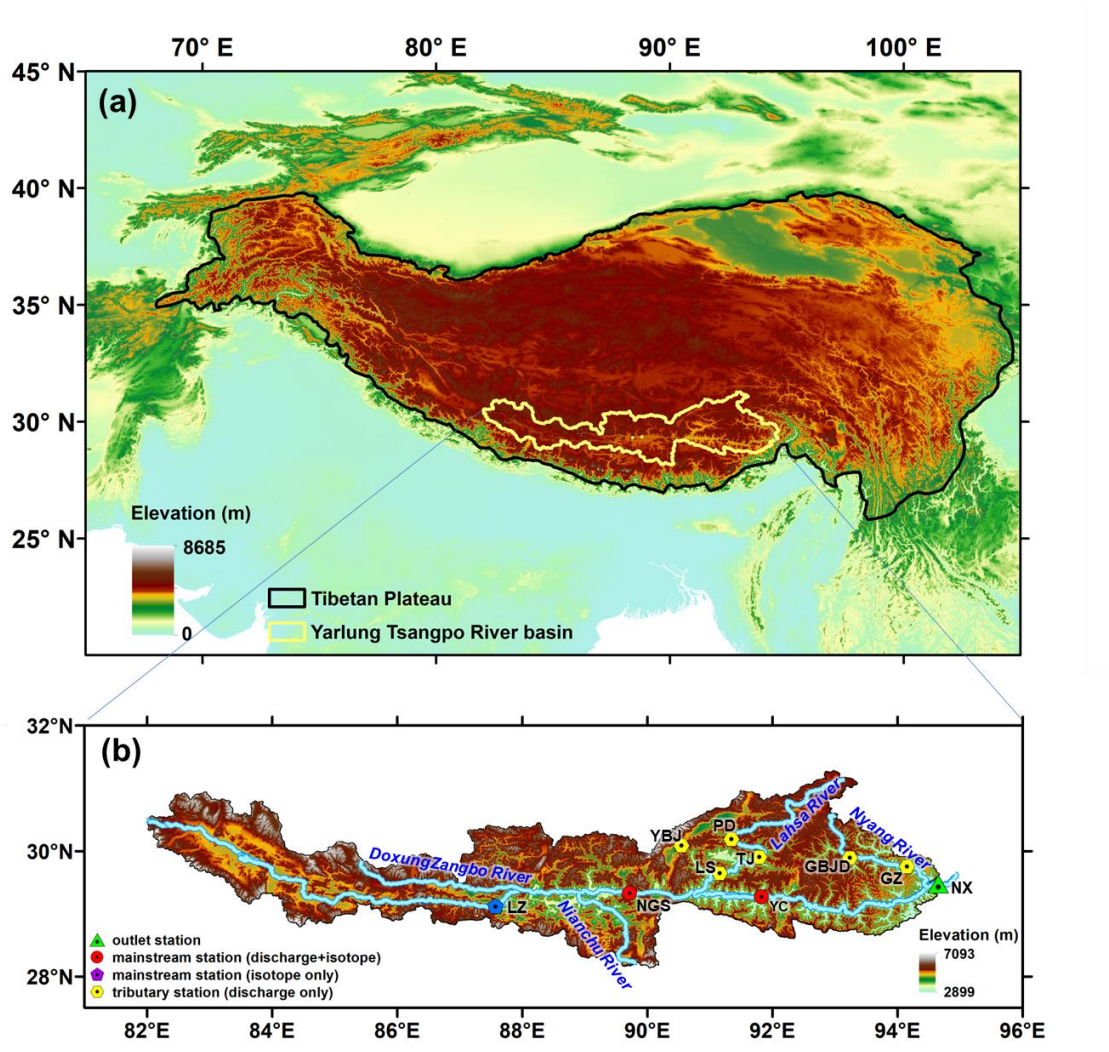


**Figure 1.** Locations and topography of (a) the Tibetan Plateau and (b) the Yarlung Tsangpo River basin. The stations used for model validation are shown in Figure (b). The abbreviations

NX, YC, NGS, LZ, GZ, GBJD, LS, TJ, PD and YBJ represent Nuxia, Yangcun, Nugesha, Lazi, Gengzhang, Gongbujiangda, Lahsa, Tangjia, Pangduo and Yangbajing stations, respectively.

**2.2 Data**

The 30 m resolution digital elevation model (DEM) data for the YTR basin was extracted from the Geospatial Data Cloud (https://www.gscloud.cn). Daily precipitation, temperature, and potential evapotranspiration data were extracted from the China Meteorological Forcing Dataset (CMFD, Yang and He, 2019) with 0.1° resolution. For the cryospheric processes, the Tibetan Plateau Snow Cover Extent (TPSCE) product (Chen et al., 2018) and the second glacier inventory dataset of China (Liu, 2012) were adopted to denote the snow and glacier coverage. The yearly glacier elevation change data with 0.5° resolution developed by Hugonnet et al. (2021) was used to represent the glacier mass balance. For the underlying conditions, the MODIS leaf area index (LAI) product MOD15A2H (Myneni et al., 2015) and normalized difference vegetation index (NDVI) product MOD13A3 (Didan, 2015) were adopted to represent the vegetation coverages, and the Harmonized World Soil Database (HWSD, He, 2019) was used to estimate the soil property parameters. Daily streamflow data at nine stations were collected (Figure 1 and Table 1).

**Table 1**. The name, location and data period of the hydrological stations

| Station | Mainstream/tributary | Period |
|---|---|---|
| Nuxia | Mainstream | 1991~2015 |
| Yangcun | Mainstream | 2001~2010 |
| Nugesha | Mainstream | 2001~2010 |
| Gengzhang | Nyang river | 2001~2015 |
| Lhasa | Lhasa river | 2001~2015 |
| Gongbujiangda | Nyang river | 2006~2009, wet season |
| Yangbajing | Lhasa river | 2006~2015, wet season |
| Pangduo | Lhasa river | 2001~2015, wet season |
| Tangjia | Lhasa river | 2001~2015, wet season |

Grab samples of precipitation and stream water were collected in 2005 at four stations along the mainstream of YTR, i.e., Lazi, Nugesha, Yangcun, and Nuxia, from upstream to downstream, for isotope analysis (Table 2, Liu et al., 2007). The outputs of Scripps Global Spectral Model with isotope incorporated (isoGSM, Yoshimura et al., 2008) with 1.875° resolution were extracted to represent the spatiotemporal variation of precipitation isotope in the YTR basin. According to our previous assessment based on the measurement precipitation

isotope data, the isoGSM captured the seasonality of precipitation isotope well, but had systematic overestimation biases in the YTR basin, which were highly correlated to the altitude (Nan et al., 2021a). The corrected isoGSM in the YTR basin produced by Nan et al. (2022) was adopted in this study.

**Table 2.** Summary of measurement isotope data in the YTR basin during 2005

| Station | Period | Precipitation | | | Stream | | |
|---|---|---|---|---|---|---|---|
| | | Number of samples | $\overline{\delta^{18}O}$ (‰) | SD (‰) | Number of samples | $\overline{\delta^{18}O}$ (‰) | SD (‰) |
| Nuxia | 14 Mar. – 23 Oct. | 86 | -10.33 | 7.18 | 34 | -15.74 | 1.60 |
| Yangcun | 17 Mar. – 5 Oct. | 59 | -13.17 | 7.10 | 30 | -16.57 | 1.69 |
| Nugesha | 14 May. – 22 Oct. | 45 | -14.29 | 7.99 | 25 | -17.84 | 0.99 |
| Lazi | 6 Jun. – 22 Sep. | 42 | -17.41 | 5.75 | 22 | -16.52 | 1.43 |

## 2.3 The tracer-aided hydrological model

A distributed tracer-aided hydrological model, Tsinghua Representative Elementary Watershed-Tracer-aided version (THREW-T) model, developed by Tian et al. (2006) and Nan et al. (2021b), was adopted to simulate the hydrological and isotopic processes in the YTR basin. The model uses the representative elementary watershed (REW) method for spatial discretization of basins, dividing the whole catchment into REWs based on DEM data. Each REW is further divided into two vertically distributed layers (i.e., surface and subsurface layers), including eight subzones (i.e., surface layer: vegetation zone, bare zone, main channel reach zone, sub stream network zone, snow-covered zone, and glacier-covered zone; subsurface layer: unsaturated zone and saturated zone) (Reggiani et al., 1999; Tian et al., 2006). This study divided the YTR basin into 297 REWs, with an average area of 694 $km^2$, ranging from 162 to 2753 $km^2$. More model details are provided in Tian et al. (2006).

A cryospheric module representing the evolutions of snowpack and glacier was incorporated into the model for application in cold regions. The total precipitation was partitioned into liquid and solid precipitation according to a temperature threshold, which was set as 0℃. The degree-day factor method was used to calculate the meltwater. The snow water equivalent of each REW was updated based on the snowfall (i.e., the solid precipitation) and the snowmelt, and the snow cover area was then determined by the snow cover depletion curve (Fassnacht et al., 2016). To simulate the evolution of glaciers, each REW is further divided into

several elevation bands to represent the change in temperature and precipitation along the altitudinal profile. The glacier within the intersection of each REW and elevation band is regarded as the representative unit for glacier simulation, similar to the discretization strategy adopted by Luo et al. (2013). For each glacier simulation unit, the model simulates the processes including the accumulation and melt of snow over glacier, the turnover of snow to ice, and the ice melt. More details and equations of the cryospheric module are provided in Nan et al. (2021b) and Cui et al. (2023).

The tracer module was incorporated into the model to simulate the isotope composition of multiple water bodies. The Rayleigh equation was adopted to simulate the isotope fractionation during water evaporation and snowmelt processes (He et al., 2019; Hindshaw et al., 2011). The isotope composition of glacier meltwater was assumed to be constantly more depleted than the local precipitation isotope and was estimated by an offset parameter (Nan et al., 2022). The isotope compositions in each simulation unit were calculated based on the complete mixing assumption. The isotope composition of snowpack and snowmelt was updated based on the water and isotope mass balance of the snowpack, similarly with other water storages. Forced by the precipitation isotope composition, the model can simulate the isotope composition of all water bodies, including stream water, soil water, groundwater, and snowpack. More details and calculation equations of the tracer module are provided in Nan et al. (2021b).

The THREW-T model quantified the contributions of multiple runoff components based on the flow-pathway definition as reviewed by He et al. (2021a). The runoff was firstly divided into surface runoff and subsurface runoff (baseflow) based on the runoff generation pathway. The surface runoff was then further divided into three components induced by different water sources (rainfall, snowmelt, and glacier melt). As a result, the total runoff was divided into four components: subsurface runoff, rainfall overland runoff, snowmelt overland runoff, and glacier melt overland runoff.

### 2.4 Model calibration and evaluation

The model was run for 25 years starting from 1991 to 2015, and was calibrated toward four objectives: the discharge at Nuxia station from 2001 to 2015, the snow cover area (SCA) from 2001 to 2015, the average glacier mass balance (GMB) from 2001 to 2010 in the whole

YTR basin, and the stream water isotope at the four stations in 2005. The Nash-Sutcliffe efficiency (NSE) was set as the evaluation metric for objectives with strong seasonality (discharge and isotope), and the root mean square error (RMSE) was set as the evaluation metric for objectives with essentially fluctuations (SCA and GMB) (Schaefli and Gupta, 2007). The optimization objective function of calibration procedure was calculated by combining the function of each objective with equal weights.

An automatic algorithm, the Python Surrogate Optimization Toolbox (pySOT, Eriksson et al., 2019) were adopted for model calibration. The pySOT algorithm uses radial basis functions (RBFs) as surrogate models to approximate the simulations, reducing the time for each model run. The symmetric Latin hypercube design (SLHD) method was used to generate parameter values, allowing an arbitrary number of design points. In each optimization run, the procedure stopped when a maximum number of allowed function evaluations was reached, which was set as 3000. In this study, the pySOT algorithm was repeated for 100 times, and a final parameter set was selected from the calibrated parameter sets manually based on the overall performance on multiple objectives. The physical basis, reference ranges and calibrated values of the calibrated parameters in the THREW-T model are shown in Table 3.

Apart from the calibration functions, the model performances were additionally evaluated by four statistical metrics: logarithmic NSE (lnNSE), RMSE-observations standard deviation ratio (RSR), Percent bias (PBIAS) and correlation coefficient (CC). The discharge simulation was evaluated by lnNSE to examine the simulation of baseflow process. Our previous studies indicated that the discharge simulation performance during validation was highly correlated with that of calibration period, partly due to the strong linearity of precipitation-discharge relation in such a large basin, but large uncertainties existed in the discharge simulation at internal stations even when the discharge at outlet station was simulated well (Nan et al., 2021b, 2022). Consequently, we not only conducted temporal validation based on the discharge data at Nuxia station during 1991~2000, but also collected additional discharge data at eight internal stations to assess the spatial consistency of model performance. The RMSE and CC of the cumulative glacier mass balance since the beginning of simulation period were also calculated to assess the glacier simulation, considering the temporal interpolation adopted by Hugonnet et al. (2021) which led to uncertainty in the year scale data.

$$\mathrm{NSE} = 1 - \frac{\sum(X_o - X_s)^2}{\sum(X_o - \overline{X_o})^2} \quad (1)$$

$$\mathrm{lnNSE} = 1 - \frac{\sum(\ln(X_o) - \ln(X_s))^2}{\sum(\ln(X_o) - \overline{\ln(X_o)})^2} \quad (2)$$

$$\mathrm{RMSE} = \sqrt{\frac{\sum(X_o - X_s)^2}{n}} \quad (3)$$

$$\mathrm{RSR} = \frac{\mathrm{RMSE}}{\mathrm{STD_{obs}}} = \frac{\sqrt{\sum(X_o - X_s)^2}}{\sqrt{\sum(X_o - \overline{X_o})^2}} \quad (4)$$

$$\mathrm{PBIAS} = \frac{\sum(X_o - X_s) * 100}{\sum X_o} \quad (5)$$

$$\mathrm{CC} = \frac{\sum[(X_s - \overline{X_s})(X_o - \overline{X_o})]}{\sqrt{\sum[(X_s - \overline{X_s})^2 (X_o - \overline{X_o})^2]}} \quad (6)$$

where, $X_s$, $X_o$, $\overline{X_s}$ and $\overline{X_o}$ are the simulated, observed, mean of simulated and mean of observed hydrological variables, respectively, and $n$ is the number of data.

**Table 3.** Physical descriptions, reference ranges and calibrated values of the calibrated parameters in the THREW-T model

| Symbol | Unit | Description | Reference range | Calibrated value |
|---|---|---|---|---|
| WM | cm | Tension water storage capacity used to calculate the saturation area | 0~10 | 2.92 |
| B | - | Shape coefficient used to calculate the saturation area | 0~1 | 0.04 |
| KKA | - | Exponential coefficient to calculate the subsurface runoff outflow rate | 0~6 | 5.92 |
| KKD | - | Linear coefficient to calculate the subsurface runoff outflow rate | 0~0.5 | 0.21 |
| $DDF_S$ | Mm/°C/d | Degree day factor for snowmelt | 0~10 | 2.60 |
| $DDF_G$ | Mm/°C/d | Degree day factor for glacier melt | 0~10 | 1.51 |
| $T_0$ | °C | Temperature threshold above which snow and glaciers melting occurs | -5 ~ 5 | -4.28 |
| $C_1$ | - | Coefficient to calculate concentration process using the Muskingum method | 0~1 | 0.04 |
| $C_2$ | - | Coefficient to calculate concentration process using the Muskingum method | 0~1 | 0.80 |

## 2.5 Perturbed climatic scenarios design

Daily temperature and precipitation data extracted from the CMFD dataset were set as the reference climate inputs. Linearly perturbed temperature and precipitation time series were adopted to represent the potential climate change ranges. Perturbed temperature input data was generated by adding one-degree increments to the reference daily temperature. The maximum

temperature increase was set as 5 ℃, because the temperature in the YTR basin is projected to increase at 1℃/20 yrs, and will increase by about 5 ℃ until the end of this decade (Cui et al., 2023). The influence of changing temperature on the potential evapotranspiration was estimated by the regression between the two factors (Eq. 7) which was developed by Van Pelt et al. (2009) and widely adopted in the projection of potential evapotranspiration (e.g., Xu et al., 2019; Cui et al., 2023).

$$\mathrm{E_p} = [1 - \alpha_0(\mathrm{T} - \overline{\mathrm{T_0}})] \cdot \overline{\mathrm{E_{p0}}} \quad (7)$$

where, $\overline{\mathrm{T_0}}$ and $\overline{\mathrm{E_{p0}}}$ are the mean daily temperature and potential evapotranspiration in each REW during the simulation period, respectively. T is the daily temperature generated by the perturbation method. $\alpha_0$ is determined by regressing the input daily potential evapotranspiration and temperature in each REW.

Perturbed precipitation input data was generated by multiplying the reference daily precipitation data from 80% to 120% with an increment of 10%, similar to Su et al. (2023) which analyzed the runoff change of three basins on the TP under hypothesized climate change scenarios. Simulation during 2001~2015 was set as the reference scenario, because the data of most objectives/stations were available during this period. In total, one reference simulation, five simulations of perturbed temperature and four simulations of perturbed precipitation were conducted. To focus on the influence of climate perturbations on the hydrological processes, the changes of underlying conditions such as soil and vegetation were not considered. In each scenario, the standard deviations (STD) of the simulated annual hydrological variables were calculated to represent the uncertainties introduced by natural climate variability. The t-Test analysis of paired two samples was conducted for the annual hydrological variables produced by reference scenario and each climate perturbation scenarios, to analyze the statistical significance of the changes. Apart from the basic hydrological variables, the concentration ratio (CR) and concentration period (CP) (Jiang et al., 2022a) were calculated by Eqs. 8~10 to characterize the runoff seasonality.

$$CR = \sqrt{R_x^2 + R_y^2} / \sum_{i=1}^{12} R_i \quad (8)$$

$$CP = \arctan(R_x / R_y) \quad (9)$$

$$R_x = \sum_{i=1}^{12} R_i \times \sin(\theta_i)\,;\ R_y = \sum_{i=1}^{12} R_i \times \cos(\theta_i) \quad (10)$$

where, $R_i$ is the runoff in the $i$th month, $R_x$ and $R_y$ are the resulting vectors in the direction of $x$ and $y$, respectively. $\theta_i$=360°/12×$i$=30°×$i$ ($i$=1,2,…,12).

## 3. Results

### 3.1 Model performance evaluation

Figure 2 shows the model performances on the four calibration objectives. The discharge was simulated well regarding both high flow and baseflow processes, as indicated by the high NSE (0.82) and lnNSE (0.84). The occurring times of peak flow were captured by the model, showing the consistency in the temporal dynamics of simulated and observed streamflow, but the simulated magnitudes of peak flow were slightly lower than the observation (Figure 2a), partly due to the poor abilities of precipitation products on accurately capturing the high precipitation in high elevation elevations and the amount of specific precipitation extreme events (Li et al., 2021; Jiang et al., 2022b; Xu et al., 2017). The performance of discharge simulation during validation period was similar with that of calibration period, with NSE and lnNSE of 0.80 and 0.88 respectively, as shown in Figure 2a. Nonetheless, the simulated annual runoff (302 mm/yr) was very close to the observation (303 mm/yr), indicating that the amount of total runoff was reproduced well. The simulated variation of SCA was smoother than the observation, but the seasonality was captured well, i.e., decreasing sharply in May and remaining extremely low from July to September (Figure 2b). The low RMSE (<0.1) suggested that the model performed well on simulating the snow processes. The model successfully simulated the declining glacier (Figure 2c), with an extremely high CC for the cumulative glacier mass balance (~1). The model estimated the annual GMB in the YTR basin as -0.545 m/yr, very close to the value extracted from the dataset of Hugonnet et al. (2021) (-0.554 m/yr). The calibrated melting temperature threshold was rather low (-4.28℃), which was partly due to the fact that melting processes were simulated at the daily step. The model simulated the variation of stream isotope well, indicated by the high NSE, CC and low PBIAS, which provided confidence in the partitioning among different runoff components (Nan et al., 2021a; He et al., 2019). The seasonality of the isotope was adequately captured: getting enriched in May, reaching maximum in June, and getting depleted in late June/early July (Figure 2d). The fact that the model simultaneously satisfied four calibration objectives ensured the proper

representation of the hydrological and cryospheric processes, and provided a reasonable baseline for the sensitivity analysis.

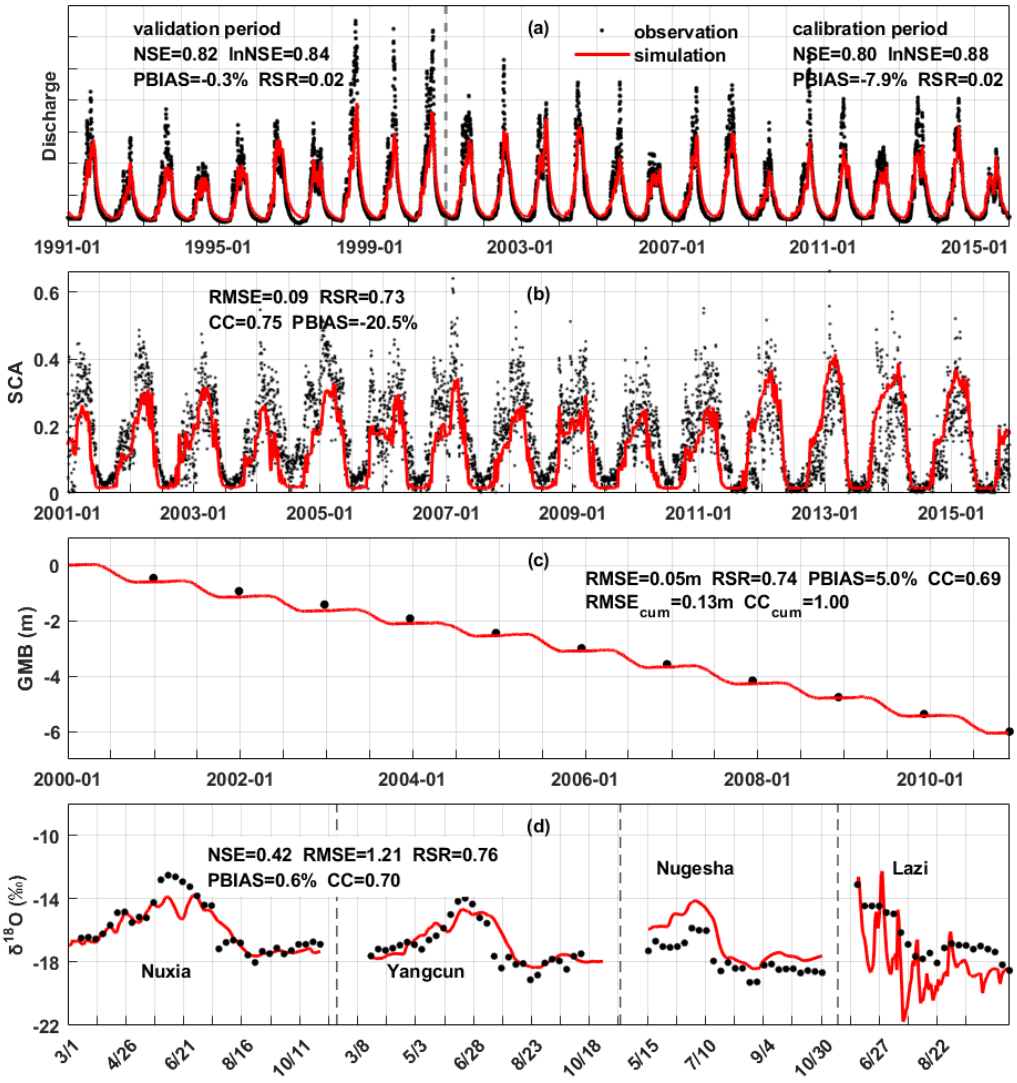


**Figure 2.** The model performances on the calibration objectives. (a) the streamflow discharge at Nuxia station, (b) the snow cover area ratio in the YTR basin, (c) the average glacier mass balance in the YTR basin, and (d) the stream water isotope at four stations in 2005.

Figure 3 shows the streamflow simulation at eight internal stations. The performance ratings were evaluated based on four metrics following the guideline by Moriasi et al. (2007). At the two stations located along the mainstream (Yangcun and Nugesha), the high flow processes were simulated well as indicated by the high NSE, but the baseflows were overestimated (Figure 3a and b). In contrast, the high flow processes were underestimated at Gengzhang station, but the baseflows were reproduced well (Figure 3c). The model produced fair performance on both high flow and baseflow simulation at Lhasa station, showing moderate

NSE and lnNSE (Figure 3d). For the four stations where only the data during the wet season were available, the PBIASs were at good levels (within ±15%) except for Gongbujiangda station (Figure 3e-h). Overall, the streamflow simulations at internal stations were not as good as the calibrated outlet station, but were at acceptable levels, as indicated by at least one satisfactory metric except for Gongbujiangda station. The high flow processes and runoff amount were reproduced relatively well, as indicated by the generally satisfactory NSE and PBIAS. But the small time-scale fluctuations and extremes were mostly not captured well, because the model was not evaluated toward metrics related to hydrological signatures (McMillan et al., 2017; Majone et al., 2022; Fenicia et al., 2018). Nonetheless, the validation based on the internal stations gave confidence in the spatial pattern of the hydrological processes and their sensitivities to the perturbed climate.

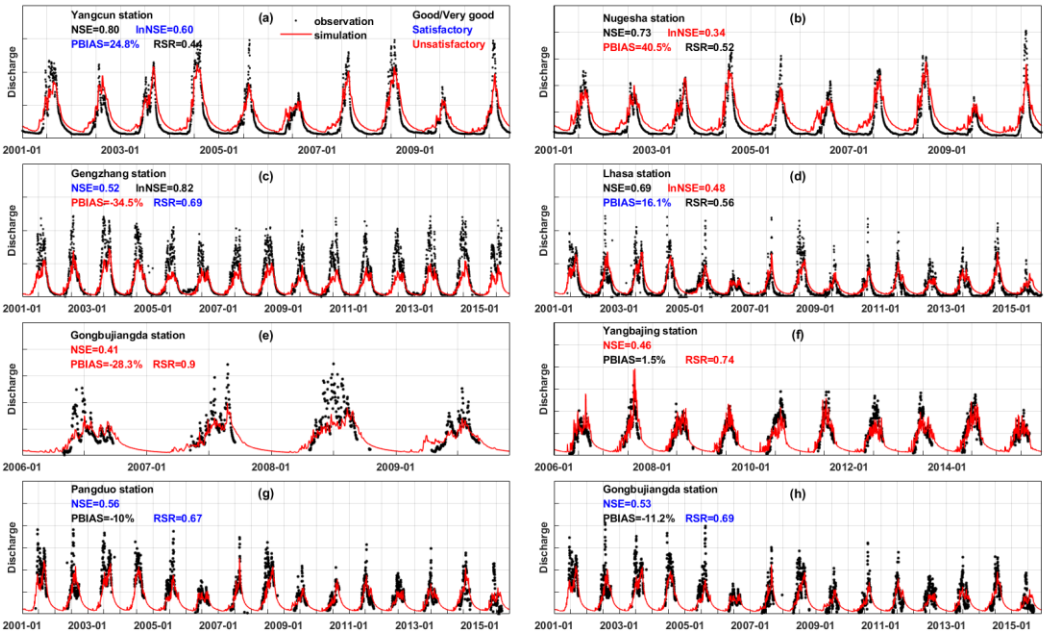


**Figure 3.** The model performances on the streamflow simulation at the internal stations.

### 3.2 Sensitivities of hydrological variables to perturbed temperature and precipitation

The sensitivities of annual runoff, snow cover area, and glacier mass balance to perturbed temperature and precipitation are shown in Figure 4. The relationships between hydrological variables and precipitation/temperature showed strong linearity, which was similar with Su et al. (2023) analyzing the hydrological sensitivities in three other large basins on the TP (~$10^5$ $km^2$), but was different from He et al. (2021b) which conducted a similar analysis in a small boreal forest basin in Canada (603 $km^2$). The annual runoff kept decreasing significantly with

the increasing temperature at the rate of -2 mm/℃ due to the increasing evaporation (Figure 4a). The decreasing rate got small when the temperature increase was higher than 3℃, partly because the controlling factor of evaporation changed from energy limitation to water limitation (Wang et al., 2022). The runoff change in response to increasing temperature was rather small compared to the intra-annual runoff variability. The snow cover area ratio significantly reduced with the increasing temperature at the rate of -1.5%/℃ because of the decreasing snowfall and increasing snowmelt, and would be smaller than half of the reference scenario for 5℃ of warming (Figure 4b). The glacier mass balance significantly got more negative with the increasing temperature because of the reducing accumulation and increasing meltwater, at the rate of -0.16 m/℃ (Figure 4c). Among the three variables, the glacier mass balance was the most sensitive to the warming climate, the relative change of which could be 150% for 5℃ of warming (Figure 4d). The changes of runoff, snow cover area and glacier mass balance in response to increasing temperature were all statistically significant at 0.01 significance level.

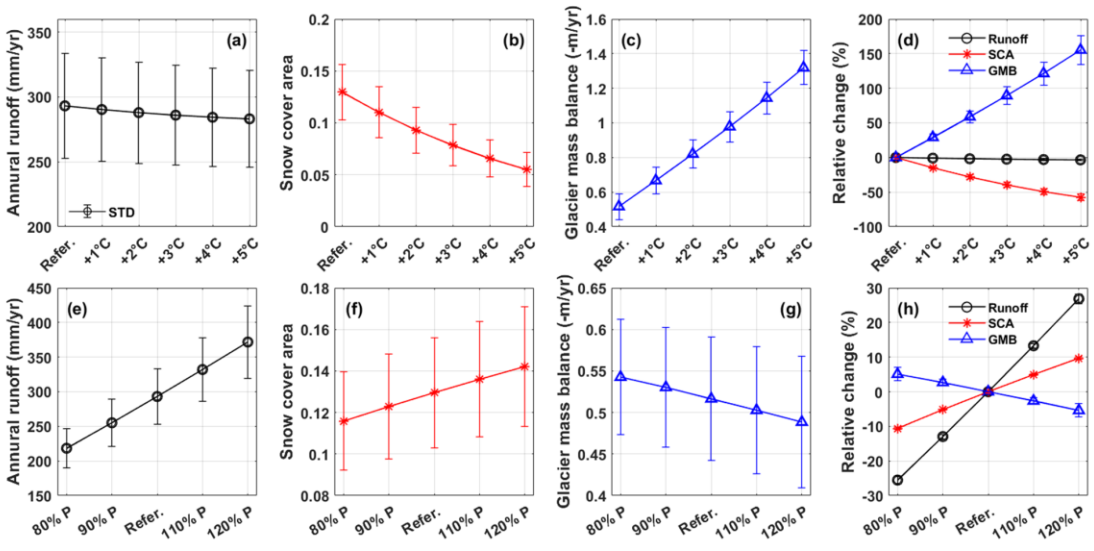


**Figure 4.** The sensitivities of annual runoff, snow cover area, and glacier mass balance to the perturbed temperature (a-d) and precipitation (e-g). Subplots (d) and (h) are the relative changes of runoff, SCA and GMB compared to the reference scenario.

The hydrological sensitivities to perturbed precipitation were opposite to that of temperature. The annual runoff increased at the rate of 38.4 mm/10% with the increasing precipitation (Figure 4e). The relative change in runoff was larger than precipitation (Figure 4h), indicating an increasing runoff coefficient with increasing precipitation. This also indicated

a small relative change in evaporation in response to precipitation perturbation, again suggesting that the energy limitation played more important role than water limitation on evaporation in the reference scenario. With the increasing precipitation, the snow cover area increased at 0.7%/10%, and the glacier mass balance got more positive at 0.014m/10% because of the larger amount of snowfall and snow/ice accumulation (Figure 4f and 4g). Among the three variables, the runoff had the highest sensitivity to perturbed precipitation, with a relative change rate of 13%/10% (Figure 4h), while the changes of snow cover area and glacier mass balance were within the range of ±10% when precipitation changed by 20%. The changes of runoff, snow cover area and glacier mass balance in response to perturbed precipitation were all statistically significant at 0.01 significance level.

### 3.3 Sensitivities of runoff variation to perturbed temperature and precipitation

The sensitivities of inter- and intra-annual runoff variation to perturbed temperature and precipitation are shown in Figure 5. The average monthly runoff were calculated based on the simulated hydrographs during the entire simulation period, and the inter-annual runoff variation was represented by the STD. The change of inter-annual runoff variation was consistent with that of total runoff. The inter-annual runoff variations were also lower in the scenarios with less runoff (increasing temperature or decreasing precipitation), showing the narrower ranges of the error bars in Figure 5a-b, and vice versa. Despite the decreasing runoff caused by increasing temperature, the average runoff for 5℃ of warming was still much higher than the lower error bar of the reference scenario (Figure 5a), suggesting that the runoff change tendency caused by the increasing temperature was relatively small compared to the inherent runoff variability. On the contrary, when precipitation increased by 20%, the average annual runoff was higher than the runoff in wet years of reference scenario (Figure 5b), indicating that the trend of precipitation change had a larger influence on the runoff than the inter-annual variation of precipitation.

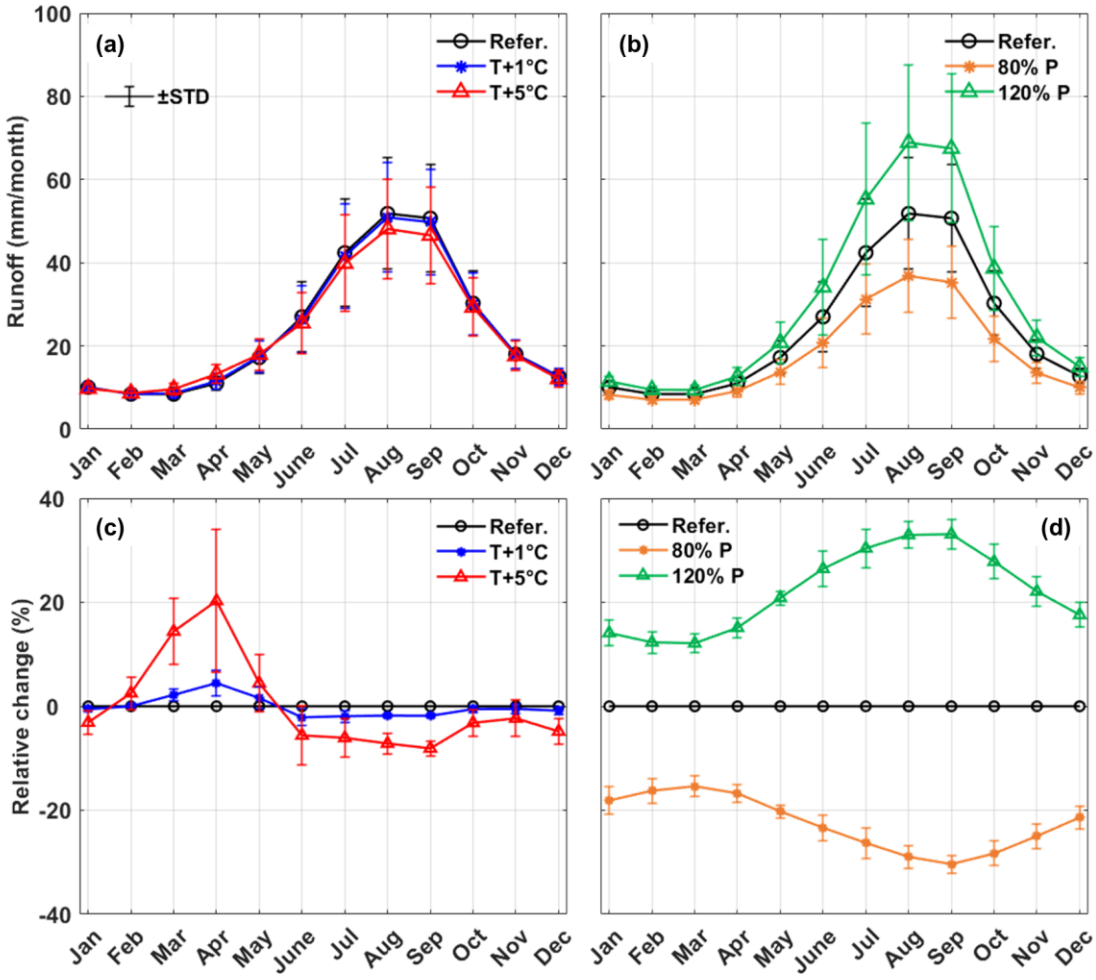


**Figure 5.** Sensitivities of intra- and inter-annual streamflow variability to the perturbed temperature and precipitation. (a) and (b) monthly runoff, (c) and (d) relative change of monthly runoff.

The sensitivities of monthly runoff were different among months. Although increasing temperature led to a decrease in the total runoff, it caused an increasing spring runoff. The monthly runoff in April increased most significantly, which increased 20% for 5°C of warming (Figure 5e). This could be attributed to the increasing snowmelt, because the SCA decreased significantly during the same period (Figure 2b). The monthly runoff in all twelve months changed accordingly to perturbed precipitation, but the change during wet seasons (August to October) was the most significant (Figure 5f). The different monthly runoff sensitivities in response to perturbed temperature and precipitation indicated that temperature changes influenced more on baseflow, while precipitation changes had higher impact on high flow processes. As a result, increasing temperature caused a more even distribution of monthly

418 runoff, while increasing precipitation had the opposite effect. The CR decreased from 0.432 to
419 0.402 for the warming of 5℃, indicating a more even seasonal runoff distribution caused by
420 increasing temperature. The CP decreased by around two days, indicating that climate warming
421 would result in advance of maximum runoff. On the contrary, the CR changed from 0.398 to
422 0.465 when precipitation increased from 80% to 120% of the reference, indicating that
423 increasing precipitation made the distribution of runoff more concentrated. The CP advanced
424 by 2.2 days in response to a 20% decreasing precipitation, but only recessed by 0.3 days in
425 response to an increasing precipitation with the same magnitude. The change of CR was
426 significant at significance level of 0.01 in all scenarios, but the change of CP was insignificant
427 in some scenarios, including T +1℃, 110% P and 120% P, with p value of 0.014, 0.02 and 0.12,
428 respectively.

429 **Table 4.** The concentration ratio (CR) and concentration period (CP) of runoff in different
430 scenarios with perturbed temperature and precipitation

| | | CR | | CP (days) | |
|---|---|---|---|---|---|
| | | Average | STD | Average | STD |
| Reference scenario | | 0.432 | 0.044 | 244.4 | 7.09 |
| T scenario | +1℃ | 0.425 | 0.044 | 244.1 | 7.12 |
| | +2℃ | 0.419 | 0.045 | 243.8 | 7.18 |
| | +3℃ | 0.413 | 0.045 | 243.3 | 7.26 |
| | +4℃ | 0.408 | 0.046 | 242.8 | 7.36 |
| | +5℃ | 0.402 | 0.046 | 242.3 | 7.45 |
| P scenario | 80% | 0.398 | 0.039 | 242.2 | 6.86 |
| | 90% | 0.415 | 0.042 | 243.6 | 7.01 |
| | 110% | 0.449 | 0.045 | 244.7 | 7.13 |
| | 120% | 0.465 | 0.045 | 244.7 | 7.14 |

431 **3.4 Sensitivities of runoff components to perturbed temperature and precipitation**

432 The contributions of runoff components in the YTR basin under scenarios with different
433 temperature and precipitation are shown in Figure 6. In the reference scenario, the subsurface
434 runoff was the dominant component, contributing 67.8% to the total runoff. Among the three
435 surface runoff components, rainfall was the dominant water source contributing 21.6% to the
436 total runoff. Glacier melt overland runoff had considerable contribution to the runoff which
437 contributed 7.4% to the total runoff, while the contribution of snowmelt overland runoff was
438 only 3.2%. The annual subsurface runoff was 195.8mm/yr (39.2 $km^3$/yr), close to the amount

(30 km$^3$/yr) estimated by Yao et al. (2021) with the groundwater model MODFLOW. It should be noted that in our model all the glacier meltwater was assumed to generate surface runoff directly because of the impermeable glacier surface, while the snowmelt was assumed to be partitioned into two components (infiltration and surface runoff) (Nan et al., 2021b, 2023; Schaefli et al., 2005).

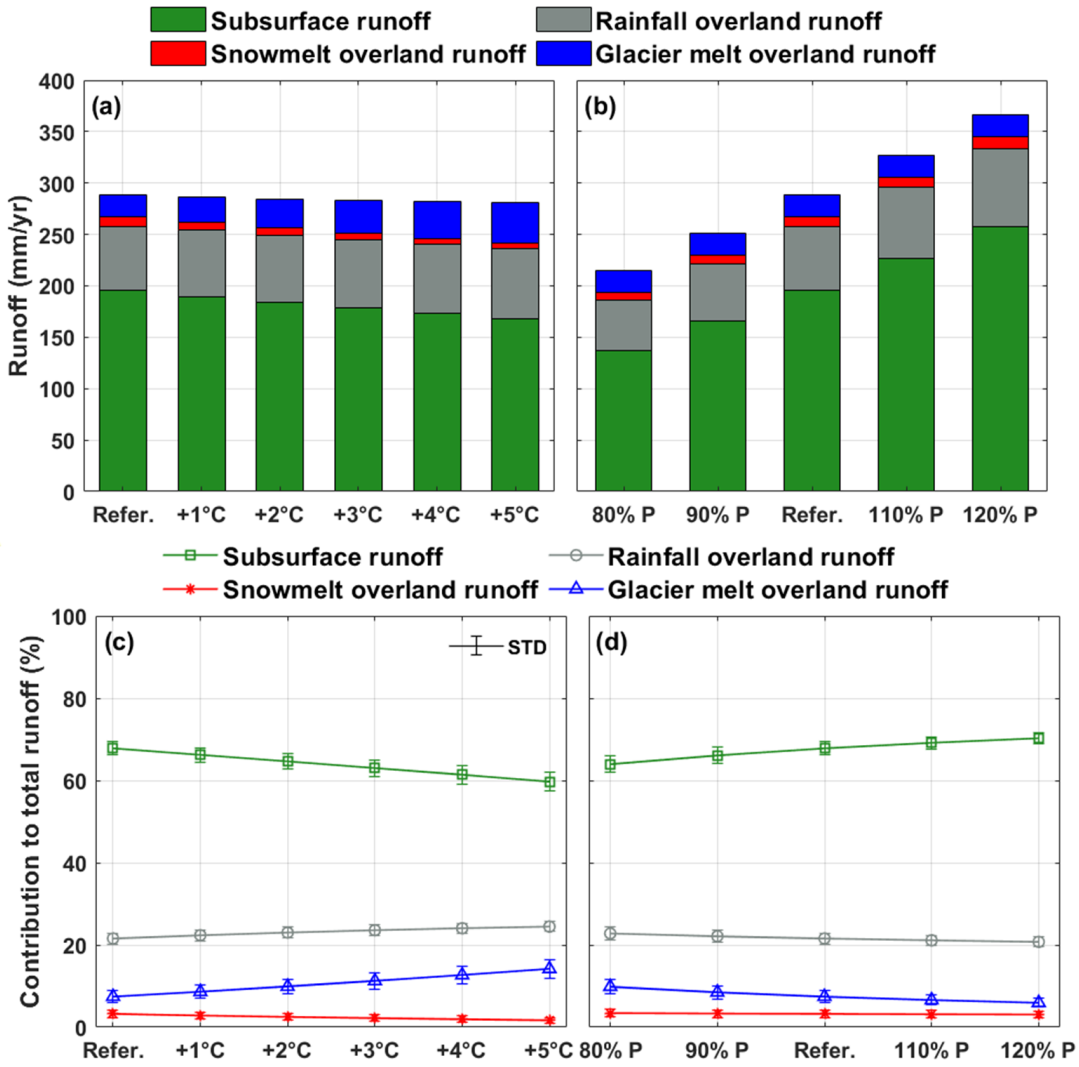


**Figure 6.** Sensitivities of the runoff components to perturbed temperature and precipitation. (a) and (b) amounts of runoff components, (c) and (d) contributions of runoff components to the total runoff.

With the increasing temperature, the amount and proportion of subsurface runoff decreased at -5.6mm/°C and -1.6%/°C, because climate warming increased evaporation and consequently reduced the subsurface water storage and outflow. The rainfall and snowmelt overland runoff increased at 1.3mm/°C (0.6%/°C) and decreased at -0.9mm/°C (-0.3%/°C), respectively,

because more rainfall was partitioned from total precipitation due to higher temperature. The glacier melt overland runoff increased significantly at 3.7mm/°C (1.4%/°C) with the increasing temperature, and the contribution to total runoff could be around 15% for 5°C of warming. The amount of all four runoff components increased with the increasing precipitation (Figure 6b), with rates of 30.1mm/10%, 6.8mm/10%, 1.0mm/10% and 0.1mm/10% for subsurface, rainfall overland, snowmelt overland and glacier melt overland runoff, respectively. However, only the proportion of subsurface runoff increased at 1.6%/10% with the increasing precipitation, while the proportions of three other components all decreased, with rates of -0.5%/10%, -0.1%/10% and -1.0%/10% for rainfall overland, snowmelt overland and glacier melt overland runoff, respectively (Figure 6d), because there was a much higher increase in the total runoff. Overall, the contributions of runoff components were more sensitive to temperature perturbation than precipitation perturbation.

Figure 7 and Tables S1-S4 show the runoff components in different seasons and their sensitivities to perturbed climate. The subsurface runoff was the dominant component in all four seasons in the reference scenario, with contribution ranging from 53% in summer to 99% in winter. The contribution of snowmelt overland runoff was extremely low in the seasons except for spring because of the small SCA in summer and autumn and the low temperature in winter. The contribution of snowmelt overland runoff in spring was close to that of rainfall overland runoff (Figure 7e-h). The contribution of glacier melt overland runoff was around half that of rainfall overland runoff in all four seasons. With climate warming, the contribution of subsurface runoff decreased in all four seasons, while the contributions of rainfall and glacier melt overland runoff increased. The significantly increasing glacier melt and rainfall led to an increase in the total runoff in spring (Figure 7a). The contribution of snowmelt overland runoff decreased in three seasons except for winter, during which its contribution slightly increased, and got around 3% for 5°C of warming (Figure 7h). With increasing precipitation, the amounts of four components increased in all seasons (Figure 7i-l), but the contributions of components remained nearly unchanged in spring, autumn and winter (Figure 7m, o-p). The contributions of runoff components were sensitive to perturbed precipitation only in summer, during which subsurface runoff contributed more to the runoff with increasing precipitation, while the contributions of rainfall and glacier melt overland runoff decreased significantly (Figure 7n).

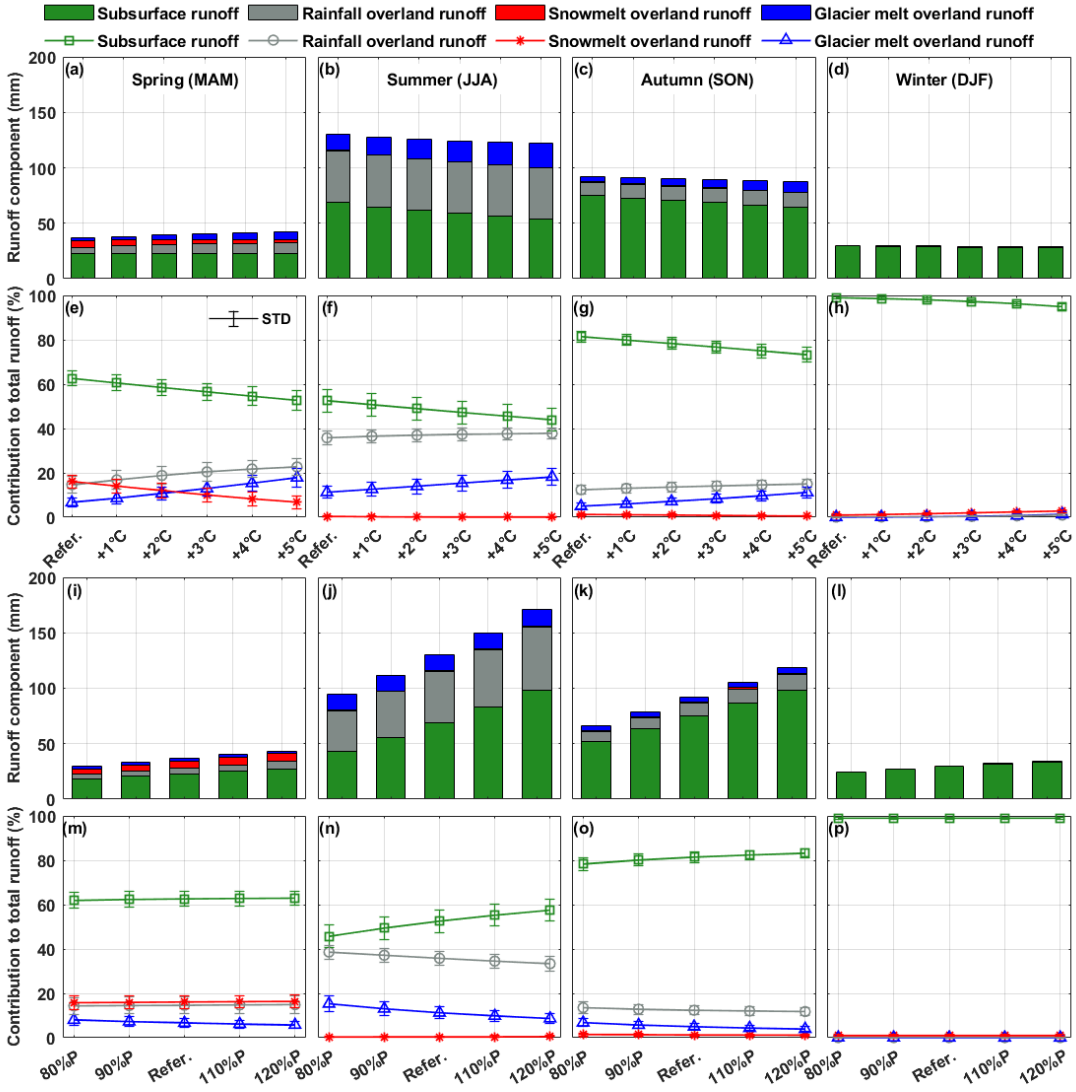


**Figure 7.** Sensitivities of the seasonal runoff components to perturbed temperature and precipitation. (a)-(d) sensitivities of amounts of runoff components to perturbed temperature, (e)-(h) sensitivities of contributions of runoff components to perturbed temperature, (i)-(l) sensitivities of amounts of runoff components to perturbed precipitation, (m)-(p) sensitivities of contributions of runoff components to perturbed precipitation.

### 3.5 Spatial pattern of local hydrological sensitivities

Considering that the YTR basin is a large basin with drainage area of $2\times10^5$ km$^2$, the spatial pattern of the local hydrological sensitivity was further analyzed with the assistance of the spatially distributed model structure. The runoff change at REW scale in four typical scenarios (i.e., 1°C of warming, 5°C of warming, precipitation changing to 80% and 120%) are shown in Figure 8. All REWs have the same runoff trend with the precipitation perturbation (Figure 8c

and 8d). The runoff increasing ranged from 12.2% to 40.4% when precipitation increased by 20%. In most REWs, the runoff changed at larger rates than precipitation, with few exceptions located in the tributaries of Nyang River, Lhasa River and the source region of mainstream, showing shallow red/blue colors in Figure 8c and 8d. On the contrary, the REW scale runoff changes in response to increasing temperature had strong spatial variability (Figure 8a and 8b). Although the runoff at the basin outlet decreased with climate warming, the REW scale runoff increased in about half of REWs. For 5℃ of warming, the REW scale runoff changes ranged from -18.6% to 54.3%. Most REWs with increasing runoff were located upstream of the mainstream, the Nianchu River, the Nyang River, and the tributary of Lhasa River (Figure 8b).

The statistical significance of runoff change in response to climate perturbation was analyzed. The runoff change in response to perturbed precipitation was significant in all the REWs, but things were different for warming temperature scenarios. The number of REWs with insignificant change trend decreased with the temperature warming level. In specify, the runoff change was insignificant (at significance level of 0.01) in 26% and 15% area of the whole basin, for the warming of 1℃ and 5℃, respectively (Figure S1). The statistical significance in response to warming temperature was related to the runoff change magnitude and drainage area (Figure S2). Consequently, although the runoff change at basin outlet was rather small (decreasing by 0.9% and 3.4% for the warming of 1℃ and 5℃, respectively), it was still statistically significant.

The runoff in some REWs changed non-monotonically with increasing temperature, i.e., the runoff change trend was reversed in different temperature intervals. Most of such non-monotonic REWs were located in the upstream region of the mainstream, with some others located in the major tributaries Nyang River, Lhasa River and Nianchu River (Figure 8e). In about 75% of non-monotonic REWs, the runoff first decreased for 1℃ of warming, and then changed to an increasing trend at higher warming levels, and the reserved trends occurred in the other 25% of REWs. The threshold temperature of trend turning differed among non-monotonic REWs, which was 3℃ in about half of the REWs. The runoff change rates in response to increasing temperature were generally low in non-monotonic REWs, most within the range of ±1%/℃.

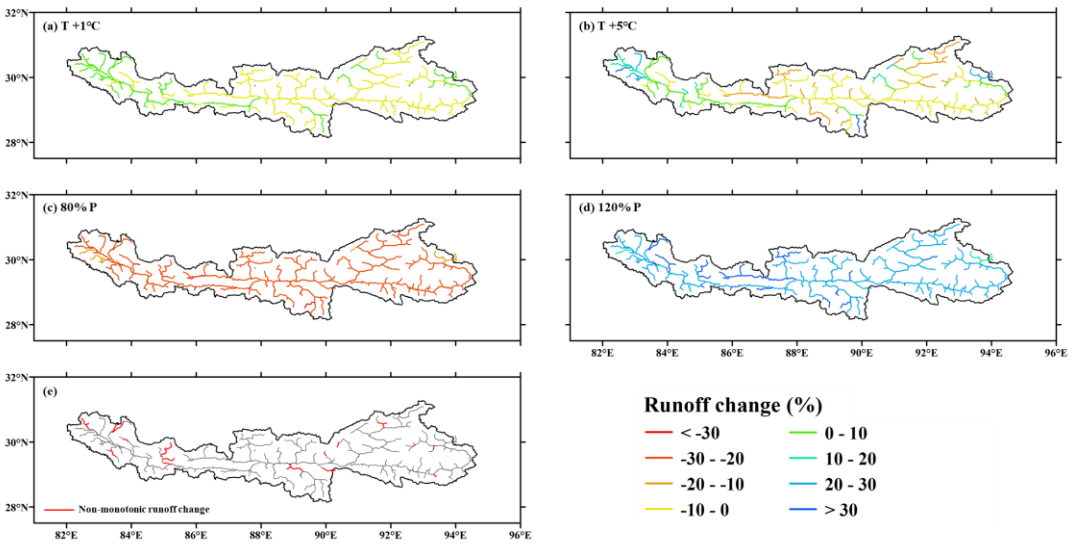


**Figure 8.** The change of REW scale runoff in response to perturbed temperature and precipitation. (a) and (b) runoff change in response to temperature perturbation, (c) and (d) runoff change in response to precipitation perturbation, (e) the locations of REWs showing non-monotonic runoff change in response to increasing temperature.

## 4. Discussions

### 4.1 The influence factors of local hydrological sensitivities: the role of glaciers

Our results show the strong spatial variability of the REW scale hydrological sensitivities to perturbed climate. Consequently, the influence factors of the local sensitivities are analyzed in this section. The basic characteristics, including mean annual temperature (MAT), mean annual precipitation (MAP), average elevation (ELE), drainage area (DRA), and glacier area ratio (GAR) were calculated for each REW as the potential factors. It should be noted that, considering the runoff concentration processes between the upstream and downstream REWs, the above characteristics were not calculated solely within each REW, but for the total drainage area controlled by each REW. The correlations between the runoff change for temperature/precipitation increasing by 5°C/20% and the potential influence factors were analyzed. The relations with the two factors with the highest coefficients are shown in Figure 9. Detailed data and relations with lower coefficients are shown in Table S5 and Figure S3.

The GAR was the most correlated factor for the hydrological sensitivities to the perturbation of both temperature and precipitation, with coefficients higher than 0.8 (Figure 9a and 9c). The runoff change for 5°C of warming increased with the increasing GAR (Figure 9a),

because of the balance between the decreasing runoff caused by evaporation and the increasing runoff contributed by glacier melt. In REWs where the GAR was higher than a threshold, the increasing glacier melt could offset the increasing evaporation, and the runoff increased with climate warming. The threshold GAR was different among REWs, ranging from 1~5%. For the REWs with GAR larger than 10%, the runoff increase for 5°C of warming could be higher than 20%. The hydrological sensitivity to increasing temperature also had a weak but significant negative correlation ($r$=-0.31, $p$<0.01) with the MAT of the REW (Figure 9b), which could be partly attributed to the interrelation between GAR and MAT, i.e., the GAR tended to be lower in warmer regions, and the runoff consequently decreased in response to increasing temperature. A lower bound of runoff change could be observed in Figure 9b for the REWs with relatively high MAT, again indicating the different limitation factors of evaporation, i.e., in relatively warm regions, the evaporation was limited by the water condition, so increasing temperature did not cause more evaporation (Wang et al., 2022).

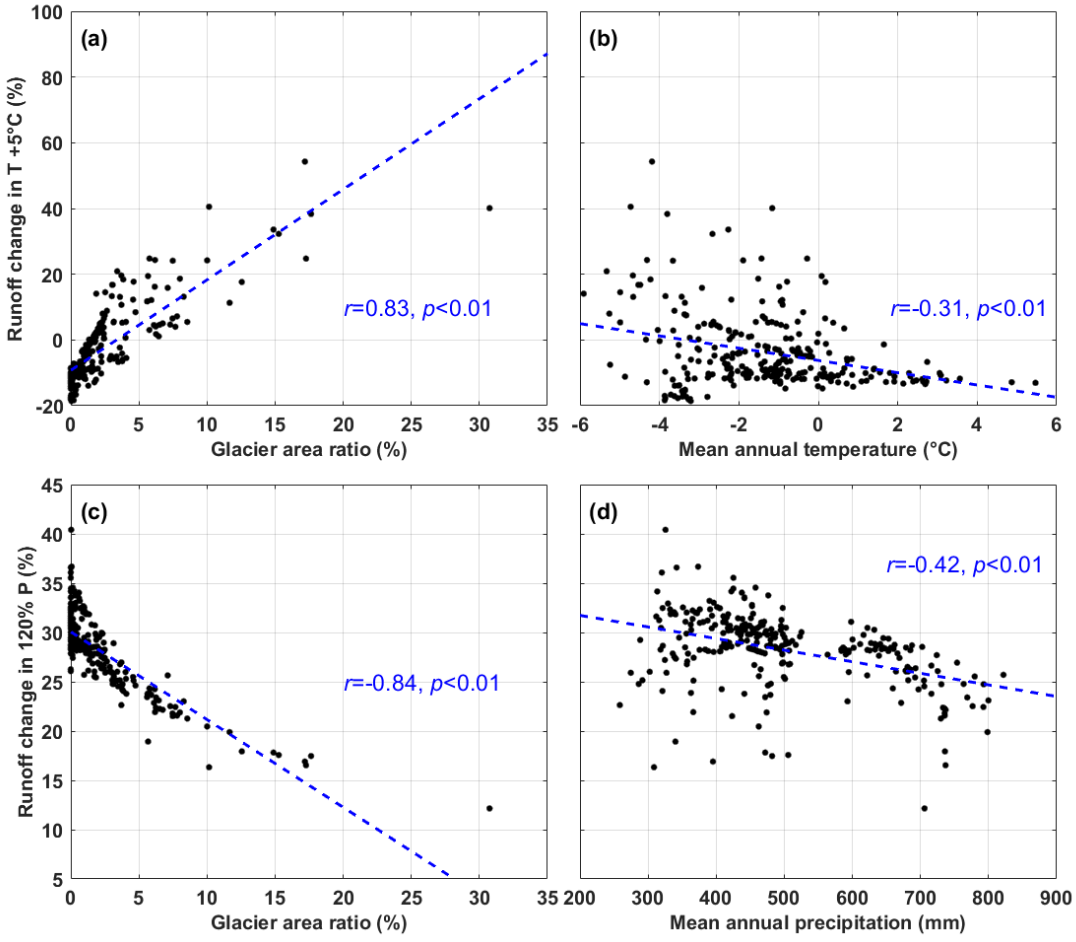


**Figure 9.** The correlations between the hydrological sensitivities to climate perturbation and

559 the dominant influence factors.

560 On the contrary, the runoff change in response to increasing precipitation had a significant
561 negative correlation ($r$=-0.84, $p$<0.01) with the GAR (Figure 9c), mainly due to the spatial
562 variability of the runoff components. In REWs with larger GAR, the contribution of
563 precipitation-induced runoff was relatively low due to the large contribution of glacier melt
564 runoff, thus the influence of increasing precipitation on runoff change was also small. It should
565 be noted that based on regression line in Figure 9c, the runoff change would be around zero in
566 regions with GAR higher than 35, which was a rather surprising inference. This might be due
567 to the small sample of REWs with high GAR based on current spatial discretization, resulting
568 in the poor confidence in the end of the regression line. The runoff change in response to
569 increasing temperature also negatively correlated with the MAP ($r$=-0.42, $p$<0.01, Figure 9d).
570 The contribution of subsurface runoff component was higher in wetter conditions (Figure 6d),
571 resulting in more evaporation and a lower runoff coefficient, which caused a relatively small
572 increase in runoff, similar with the finding by He et al. (2021b).

573 Our results indicate that the runoff in some REWs changed non-monotonically in response
574 to the increasing temperature. The characteristics of these non-monotonic REWs were further
575 analyzed. Interestingly, the GAR of non-monotonic REWs had a good linear relationship with
576 their MAP (Figure 10a). The regression equation of the linear relation was
577 GAR(%)=0.011*MAP(mm)-2.43 ($r$=0.92). Moreover, this regression line was the dividing line
578 between the REWs where runoff increased with increasing temperature and those with opposite
579 runoff trends in the GAR-MAP plot (Figure 10a). The REWs located in the upper part of the
580 plot had larger runoff increasing rates. This indicated that the local hydrological sensitivity to
581 increasing temperature was determined by the relationship between GAR and MAP. In wetter
582 REWs with larger MAP, more glaciers were needed to offset the decreasing runoff due to the
583 increasing temperature and evaporation. These findings suggested the important role of glaciers
584 in determining the runoff change in response to climate change. Similar characteristics were
585 observed in the precipitation perturbation scenarios (Figure 10b). The runoff change rate was
586 different from the precipitation change rate in all REWs, and was consistently either higher or
587 lower than precipitation change rate in most REWs. But there were three REWs shifting from

ΔQ/ΔP <1 to >1, the GAR and MAP of which also had linear relationship, forming the boundary of REWs where runoff changed more significantly than precipitation and those with lower runoff change rate. However, there were only three such non-monotonic REWs for precipitation perturbation scenarios, providing less confidence to the boundary line. As a result, there were some REWs lying lower than the boundary line but with lower runoff change rate than precipitation (Figure 10b).

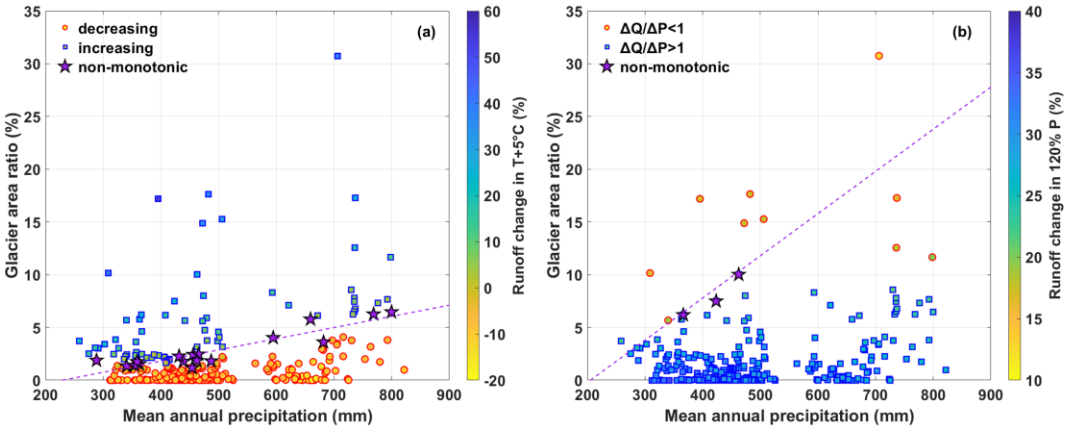


**Figure 10.** The interrelation among the REW scale glacier area ratio, mean annual precipitation and the runoff change for (a) 5°C of warming and (b) 120% precipitation.

### 4.2 Implications of the sensitivity analysis

The sensitivity analysis indicated the important role of glaciers in providing meltwater to offset the runoff decreasing caused by climate warming. Our study showed that glacier meltwater had a limited contribution to the total runoff in the YTR basin, similar with some recent studies (Wang et al., 2021; Cui et al., 2023), resulting in a decreasing runoff trend with increasing temperature. However, the spatial pattern analysis indicated that the role of glacier melt runoff could be rather significant in the regions with large area covered by glaciers. For example, the runoff increased significantly in the Yangbajing tributary of the Lhasa River in response to increasing temperature (Figure 8), consistent with previous research estimating a high contribution of glacier melt to runoff in this region (Lin et al., 2020; Wang et al., 2023). It is therefore necessary to address the spatial scale issue when discussing the role of glacier meltwater on water resources.

Several studies have stressed the important role of glaciers on the TP as the largest global store of frozen water which supplied freshwater resources to downstream regions (Yao et al.,

2022). This study quantitively estimated the role of glacier meltwater in offsetting the decreasing runoff with increasing temperature and evaporation. Our results indicated that the influences of glacier on hydrological processes were highly dependent on the spatial scale and the local meteorological characteristics. Specifically, the role of glacier meltwater would undoubtedly be more significant in regions with larger glacier cover areas (Luo et al., 2018; Zhao et al., 2019; Khanal et al., 2021). Meanwhile, the role of glaciers was smaller in wetter regions with higher precipitation because of the relatively low contribution of glacier meltwater in total runoff. Consequently, the regions with larger precipitation amounts but little glacier coverage would face a greater risk of water resources shortage in a warming future (Figure 10a), and other regions would face the similar condition because of the shrinking glacier area. Our results also suggested a larger influence of precipitation change on runoff than that of temperature change (Figure 4), thus an accurate projection of precipitation is crucial for the assessment of water resources under climate change. Recent studies showed a decreasing precipitation trend after 2000 in the YTR basin (Li et al., 2016; Luan and Zhai, 2022), likely posing threats of water scarcity to the riparian regions and again highlighting the important role of glacier in maintaining water resources.

Our results showed that the runoff responded to increasing temperature non-monotonically in some regions. These non-monotonic REWs represented the most dynamic regions within the basin, as they kept shifting between energy and water limited stages. Recent studies also projected the non-monotonic runoff change on the TP at increasing warming levels (Cui et al., 2023), i.e., the annual mean runoff for major rivers on the TP will significantly decrease by 0.1~3.2% at the warming level of 1.5℃, and increase by 1.5~12% at 3.0℃ in the future. Although seemingly similar, the two studies revealed two different phenomena. In particular, the non-monotonic runoff change projected by Cui et al. (2023) was driven by the output put of climatic projection data CMIP6 (Eyring et al., 2016), and the runoff change was dominated by the tendencies and periodicities of climate factors, especially precipitation (Wu et al., 2022). Our study analyzed the runoff change in response to climate warming with fixed precipitation input, and the trend was the result of the comprehensive response of multiple water balance components to climate change. The local non-monotonic hydrological sensitivity was essentially a borderline condition of increasing and decreasing trend, which reflected the

balance of increasing meltwater and evaporation in response to climate warming.

### 4.3 Limitations

This study explored the sensitivities of hydrological processes to climate change by designing temperature and precipitation perturbation scenarios, rather than projecting future runoff using the forcing data from general circulation models (GCMs). The assumed climate perturbation method is widely used in runoff projection studies (He et al., 2021b; Su et al., 2023; Rasouli et al., 2014; Rasouli et al., 2015), with the advantage of avoiding the computation cost of correcting biases and downscaling GCMs to regional scale (Piani et al., 2010; Xu et al., 2019). However, the assumed climate perturbation did not reflect the gradual process of climate change. Specifically, the temperature should go through relatively low warming levels before arriving at the assumed highest level, but the climate perturbation method actually assumed an abrupt climate change. Because of the relatively short simulation period, the potential trend turning of meltwater caused by the combined effect of increasing melting rate and shrinking glacier area cannot be reflected by the sensitivity analysis (Yao et al., 2022; Zhang et al., 2022a). We can expect that the role of glaciers when temperature increases by 5°C in the future should be less than our results, because the glacier covered area at that time will be less than the current condition (Yao et al., 2022). Meanwhile, the potential influences of temperature and precipitation change on soil and vegetation conditions (Boulanger et al., 2016) were not considered when designing the climate perturbation scenarios. Nonetheless, the simple sensitivity analysis in this study helped better understand the separate effect of changing temperature and precipitation on runoff, and informed the role of glaciers in controlling the spatial pattern of runoff change.

Another limitation comes from the uncertainties of hydrological model. Although validated by the measurement data of multiple objectives and several internal stations, the model still had potential uncertainties. First, as the most important forcing data, the common precipitation datasets in the YTR basin all had large uncertainties, due to the lack of validation data in high elevation regions (Xu et al., 2017), leading to uncertainties in hydrological simulation. The model underestimated the peak streamflow for most stations, which could be

attributed to the underestimated precipitation during wet seasons by CMFD dataset. Further correction on the precipitation product based on more station data could be helpful to remove the bias. Second, because of the complex hydrological processes and runoff components, the parameter equifinality problem usually existed in the hydrological model in large mountainous basins (Gupta et al., 2008; Nan et al., 2021a). He et al. (2019) indicated that the uncertainties of runoff component contributions could be nearly 20% even when the simulations of streamflow, snow, glacier and isotope were satisfied simultaneously. The misestimation of the runoff regime would undoubtedly influence the sensitivity analysis. Third, the calibration procedure of this work was rather simple, based on a combination of automatic algorithm and manual selection. The influences of calibration scheme, optimized objective function (Gupta et al., 2009; Majone et al., 2022) and the weights of multiple objectives (Tong et al., 2021) on hydrological sensitivities were not analyzed deeply. For instance, different types of evaluation metrics for multiple objectives were added together directly, which may result in different impacts on the integrated objective function. Lastly, the calibrated parameters were assumed to be spatially uniform within the whole basin to avoid introducing too many parameters. Although this is similar to several large-scale modeling studies (e.g., Cui et al., 2023; Lutz et al., 2014), the uniform parameter might be inadequate to represent the spatial variability of hydrological processes, which may influence some conclusions of the sensitivity analysis. For example, considering the potential spatial variability of glacier melting rate, the characteristics of non-monotonic REWs in Figure 10 may not form a straight line. Currently this work only considered the uncertainties introduced by natural climate variabilities. More works are needed in the future to analyze the parameter sensitivities and the uncertainties from calibration schemes.

## 5. Conclusions

This study adopted the tracer-aided hydrological model THREW-T in a typical large mountainous basin Yarlung Tsangpo River (YTR) on the Tibetan Plateau (TP). The model was validated against multiple objectives (streamflow, snow, glacier and isotope) and the streamflow at internal stations. The sensitivities of hydrological processes to perturbed temperature and precipitation were analyzed. The spatial pattern of local hydrological

sensitivities and the influence factors were explored. Our main findings are as follows:

(1) The THREW-T model performed well on simulating the streamflow, snow cover area (SCA), glacier mass balance (GMB), and stream water isotope, ensuring good representation of the key cryospheric processes and a reasonable estimation of the contributions of runoff components. The model performed acceptably on simulating the streamflow at eight internal stations located in the mainstream and two major tributaries, which indicated that the spatial pattern of hydrological processes was reflected by the model, and provided confidence in the sensitivity analysis.

(2) Most hydrological characteristics responded to increasing temperature and precipitation oppositely. Increasing temperature led to decreasing annual runoff, SCA and GMB, and changed the runoff variation showing a smaller inter-annual variation, a more even distributed intra-annual distribution, and an earlier maximum runoff. It also influenced the runoff regime by increasing the contributions of rainfall and glacier melt overland runoff, but decreasing the subsurface runoff and snowmelt overland runoff. Increasing precipitation had the opposite effects to increasing temperature.

(3) The distribution of local hydrological sensitivities had a strong spatial variability. The local runoff change in response to increasing temperature varied significantly, with changing rate of -18.6% to 54.3% for 5℃ of warming. The glacier area ratio (GAR) was the dominant factor of the spatial pattern of hydrological sensitivities to both perturbed temperature and precipitation. Some regions had a non-monotonic runoff change rate in response to climate perturbation, which represented the most dynamic regions within the basin, as they kept shifting between energy and water limited stages. The GAR and mean annual precipitation (MAP) of the non-monotonic regions had a linear relation, and formed the boundary of regions with different runoff trends in the GAR-MAP plot.

## Code and data availability

Code and data availability. The isotope data and the code of THREW-T model used in this study are available from the corresponding author (tianfq@tsinghua.edu.cn). Other data sets are publicly available as follows: DEM (http://www.gscloud.cn/sources/details/310?pid=302, last

access: 1 January 2019, Geospatial Data Cloud Site, 2019), CMFD (https://doi.org/10.11888/AtmosphericPhysics.tpe.249369.file, Yang and He, 2019), glacier inventory data (https://doi.org/10.3972/glacier.001.2013.db, Liu, 2012), glacier elevation change data (https://doi.org/10.6096/13, Huggonet et al., 2021), NDVI (https://doi.org/10.5067/MODIS/MOD13A3.006, Didan, 2015), LAI (https://doi.org/10.5067/MODIS/MOD15A2H.006, Myneni et al., 2015), HWSD (https://data.tpdc.ac.cn/zh-hans/data/3519536a-d1e7-4ba1-8481-6a0b56637baf/?q=HWSD, last access: 1 January 2019, He, 2019). These datasets not publicly available are referred to in the main text (Chen et al., 2018; Liu et al., 2007).

## Author contribution

YN conceived the idea and collected data; YN and FT conducted analysis and wrote the paper.


## Financial support

This study has been supported by the National Natural Science Foundation of China (grant no. 92047301) and the Shuimu Tsinghua Scholar Program.


## Competing interests

At least one of the (co-)authors is a member of the editorial board of Hydrology and Earth System Sciences.

## References


Aygun, O., Kinnard, C., Campeau, S., and Krogh, S. A.: Shifting Hydrological Processes in a Canadian Agroforested Catchment due to a Warmer and Wetter Climate, Water, 12, 10.3390/w12030739, 2020.

Bai, X. L., Zhao, W. Z., Liu, H., Zhang, Y. Y., Yang, Q. Y., Liu, J. T., and Chang, X. L.: Effects of precipitation changes and land-use alteration on streamflow: A comparative analysis from two adjacent catchments in the Qilian Mountains, arid northwestern China, Frontiers

in Environmental Science, 11, 10.3389/fenvs.2023.1097049, 2023.

Birkel, C. and Soulsby, C.: Advancing tracer-aided rainfall-runoff modelling: a review of progress, problems and unrealised potential, Hydrological Processes, 29, 5227-5240, 10.1002/hyp.10594, 2015.

Bloschl, G. and Montanari, A.: Climate change impacts-throwing the dice?, Hydrological Processes, 24, 374-381, 10.1002/hyp.7574, 2010.

Boulanger, Y., Taylor, A. R., Price, D. T., Cyr, D., McGarrigle, E., Rammer, W., Sainte-Marie, G., Beaudoin, A., Guindon, L., and Mansuy, N.: Climate change impacts on forest landscapes along the Canadian southern boreal forest transition zone, Landscape Ecology, 32, 1415-1431, 10.1007/s10980-016-0421-7, 2017.

Cao, L. G. and Pan, S. M.: Changes in precipitation extremes over the "Three-River Headwaters" region, hinterland of the Tibetan Plateau, during 1960-2012, Quaternary International, 321, 105-115, 10.1016/j.quaint.2013.12.041, 2014.

Chen, X., Long, D., Liang, S., He, L., Zeng, C., Hao, X., and Hong, Y.: Developing a composite daily snow cover extent record over the Tibetan Plateau from 1981 to 2016 using multisource data, Remote Sensing of Environment, 215, 284-299, 10.1016/j.rse.2018.06.021, 2018.

Criss, R. E. and Winston, W. E.: Do Nash values have value? Discussion and alternate proposals, Hydrological Processes, 22, 2723-2725, 10.1002/hyp.7072, 2008.

Cui, T., Li, Y., Yang, L., Nan, Y., Li, K., Tudaji, M., Hu, H., Long, D., Shahid, M., Mubeen, A., He, Z., Yong, B., Lu, H., Li, C., Ni, G., Hu, C., and Tian, F.: Non-monotonic changes in Asian Water Towers' streamflow at increasing warming levels, Nature communications, 14, 1176-1176, 10.1038/s41467-023-36804-6, 2023.

Didan, K.: MOD13A3 MODIS/Terra vegetation Indices Monthly L3 Global 1 km SIN Grid V006, NASA EOSDIS Land Processes DAAC [dataset], https://doi.org/10.5067/MODIS/MOD13A3.006, 2015.

Eriksson, D., Bindel, D., and Shoemaker, C. A.: pySOT and POAP: An event-driven asynchronous framework for surrogate optimization, arXiv preprint, 10.48550/arXiv.1908.00420, 2019.

Eyring, V., Bony, S., Meehl, G. A., Senior, C. A., Stevens, B., Stouffer, R. J., and Taylor, K. E.:

786 Overview of the Coupled Model Intercomparison Project Phase 6 (CMIP6) experimental
787 design and organization, Geoscientific Model Development, 9, 1937-1958, 10.5194/gmd-
788 9-1937-2016, 2016.
789 Fassnacht, S. R., Sexstone, G. A., Kashipazha, A. H., Ignacio Lopez-Moreno, J., Jasinski, M.
790 F., Kampf, S. K., and Von Thaden, B. C.: Deriving snow-cover depletion curves for
791 different spatial scales from remote sensing and snow telemetry data, Hydrological
792 Processes, 30, 1708-1717, 10.1002/hyp.10730, 2016.
793 Fenicia, F., Kavetski, D., Reichert, P., and Albert, C.: Signature-Domain Calibration of
794 Hydrological Models Using Approximate Bayesian Computation: Empirical Analysis of
795 Fundamental Properties, Water Resources Research, 54, 3958-3987,
796 10.1002/2017wr021616, 2018.
797 Gao, J., Yao, T. D., Masson-Delmotte, V., Steen-Larsen, H. C., and Wang, W. C.: Collapsing
798 glaciers threaten Asia's water supplies, Nature, 565, 19-21, 10.1038/d41586-018-07838-4,
799 2019.
800 Gupta, H. V., Kling, H., Yilmaz, K. K., and Martinez, G. F.: Decomposition of the mean squared
801 error and NSE performance criteria: Implications for improving hydrological modelling,
802 Journal of Hydrology, 377, 80-91, 10.1016/j.jhydrol.2009.08.003, 2009.
803 Gupta, H. V., Wagener, T., and Liu, Y.: Reconciling theory with observations: elements of a
804 diagnostic approach to model evaluation, Hydrological Processes, 22, 3802-3813,
805 10.1002/hyp.6989, 2008.
806 He, Y.: Pan-TPE soil map based on Harmonized World Soil Database (V1.2), National Tibetan
807 Plateau Data Center [dataset], 2019.
808 He, Z. H. and Pomeroy, J. W.: Assessing hydrological sensitivity to future climate change over
809 the Canadian southern boreal forest, Journal of Hydrology, 624,
810 10.1016/j.jhydrol.2023.129897, 2023.
811 He, Z., Duethmann, D., and Tian, F.: A meta-analysis based review of quantifying the
812 contributions of runoff components to streamflow in glacierized basins, Journal of
813 Hydrology, 603, 10.1016/j.jhydrol.2021.126890, 2021a.
814 He, Z. H., Pomeroy, J. W., Fang, X., and Peterson, A.: Sensitivity analysis of hydrological
815 processes to perturbed climate in a southern boreal forest basin, Journal of Hydrology, 601,

816 10.1016/j.jhydrol.2021.126706, 2021b.
817 He, Z., Unger-Shayesteh, K., Vorogushyn, S., Weise, S. M., Kalashnikova, O., Gafurov, A.,
818 Duethmann, D., Barandun, M., and Merz, B.: Constraining hydrological model parameters
819 using water isotopic compositions in a glacierized basin, Central Asia, Journal of
820 Hydrology, 571, 332-348, 10.1016/j.jhydrol.2019.01.048, 2019.
821 Hindshaw, R. S., Tipper, E. T., Reynolds, B. C., Lemarchand, E., Wiederhold, J. G., Magnusson,
822 J., Bernasconi, S. M., Kretzschmar, R., and Bourdon, B.: Hydrological control of stream
823 water chemistry in a glacial catchment (Damma Glacier, Switzerland), Chemical Geology,
824 285, 215-230, 10.1016/j.chemgeo.2011.04.012, 2011.
825 Hugonnet, R., McNabb, R., Berthier, E., Menounos, B., Nuth, C., Girod, L., Farinotti, D., Huss,
826 M., Dussaillant, I., Brun, F., and Kaab, A.: Accelerated global glacier mass loss in the early
827 twenty-first century, Nature, 592, 726-+, 10.1038/s41586-021-03436-z, 2021.
828 Immerzeel, W. W., van Beek, L. P. H., and Bierkens, M. F. P.: Climate Change Will Affect the
829 Asian Water Towers, Science, 328, 1382-1385, 10.1126/science.1183188, 2010.
830 Jiang, Y., Xu, Z., and Xiong, L.: Runoff variation and response to precipitation on multi-spatial
831 and temporal scales in the southern Tibetan Plateau, Journal of Hydrology-Regional
832 Studies, 42, 10.1016/j.ejrh.2022.101157, 2022a.
833 Jiang, Y., Yang, K., Yang, H., Lu, H., Chen, Y., Zhou, X., Sun, J., Yang, Y., and Wang, Y.:
834 Characterizing basin-scale precipitation gradients in the Third Pole region using a high-
835 resolution atmospheric simulation-based dataset, Hydrology and Earth System Sciences,
836 26, 4587-4601, 10.5194/hess-26-4587-2022, 2022b.
837 Khanal, S., Lutz, A. F., Kraaijenbrink, P. D. A., van den Hurk, B., Yao, T., and Immerzeel, W.
838 W.: Variable 21st Century Climate Change Response for Rivers in High Mountain Asia at
839 Seasonal to Decadal Time Scales, Water Resources Research, 57, 10.1029/2020wr029266,
840 2021.
841 Li, X., Yao, Z., Xiao, J., and Wang, H.: Analysis of the spatial-temporal variation characteristics
842 of precipitation over the Tibetan Plateau from 1961 through 2010, Journal of Glaciology
843 and Geocryology, 38, 1233-1240, 2016.
844 Li, C., Sinha, E., Horton, D. E., Diffenbaugh, N. S., and Michalak, A. M.: Joint bias correction
845 of temperature and precipitation in climate model simulations, Journal of Geophysical

Research-Atmospheres, 119, 13153-13162, 10.1002/2014jd022514, 2014.

Li, Z. X., Feng, Q., Li, Z. J., Yuan, R. F., Gui, J., and Lv, Y. M.: Climate background, fact and hydrological effect of multiphase water transformation in cold regions of the Western China: A review, Earth-Science Reviews, 190, 33-57, 10.1016/j.earscirev.2018.12.004, 2019.

Li, Z. J., Li, Z. X., Song, L. L., Gui, J., Xue, J., Zhang, B. J., and Gao, W. D.: Hydrological and runoff formation processes based on isotope tracing during ablation period in the source regions of Yangtze River, Hydrology and Earth System Sciences, 24, 4169-4187, 10.5194/hess-24-4169-2020, 2020.

Li, K., Tian, F., Khan, M. Y. A., Xu, R., He, Z., Yang, L., Lu, H., and Ma, Y.: A high-accuracy rainfall dataset by merging multiple satellites and dense gauges over the southern Tibetan Plateau for 2014-2019 warm seasons, Earth System Science Data, 13, 5455-5467, 10.5194/essd-13-5455-2021, 2021.

Lin, L., Gao, M., Liu, J., Wang, J., Wang, S., Chen, X., and Liu, H.: Understanding the effects of climate warming on streamflow and active groundwater storage in an alpine catchment: the upper Lhasa River, Hydrology and Earth System Sciences, 24, 1145-1157, 10.5194/hess-24-1145-2020, 2020.

Liu, S.: The second glacier inventory dataset of China (version 1.0) (2006–2011), National Tibetan Plateau Data Center [dataset], 10.3972/glacier.001.2013.db, 2012.

Liu, Z. F., Tian, L. D., Yao, T. D., Gong, T. L., Yin, C. L., and Yu, W. S.: Temporal and spatial variations of delta O-18 in precipitation of the Yarlung Zangbo River Basin, Journal of Geographical Sciences, 17, 317-326, 10.1007/s11442-007-0317-1, 2007.

Luan, L. and Zhai, P.: Changes in rainy season precipitation properties over the Qinghai-Tibet Plateau based on multi-source datasets, Progressus Inquisitiones de Mutatione Climatis, 19, 173-190, 2023.

Luo, Y., Arnold, J., Liu, S., Wang, X., and Chen, X.: Inclusion of glacier processes for distributed hydrological modeling at basin scale with application to a watershed in Tianshan Mountains, northwest China, Journal of Hydrology, 477, 72-85, 10.1016/j.jhydrol.2012.11.005, 2013.

Luo, Y., Arnold, J., Liu, S. Y., Wang, X. Y., and Chen, X.: Inclusion of glacier processes for

distributed hydrological modeling at basin scale with application to a watershed in Tianshan Mountains, northwest China, Journal of Hydrology, 477, 72-85, 10.1016/j.jhydrol.2012.11.005, 2013.

Luo, Y., Wang, X., Piao, S., Sun, L., Ciais, P., Zhang, Y., Ma, C., Gan, R., and He, C.: Contrasting streamflow regimes induced by melting glaciers across the Tien Shan - Pamir - North Karakoram, Scientific Reports, 8, 10.1038/s41598-018-34829-2, 2018.

Luo, Y., Wang, X. L., Piao, S. L., Sun, L., Ciais, P., Zhang, Y. Q., Ma, C. K., Gan, R., and He, C. S.: Contrasting streamflow regimes induced by melting glaciers across the Tien Shan - Pamir - North Karakoram, Scientific Reports, 8, 10.1038/s41598-018-34829-2, 2018.

Lutz, A. F., Immerzeel, W. W., Shrestha, A. B., and Bierkens, M. F. P.: Consistent increase in High Asia's runoff due to increasing glacier melt and precipitation, Nature Climate Change, 4, 587-592, 10.1038/nclimate2237, 2014.

Majone, B., Avesani, D., Zulian, P., Fiori, A., and Bellin, A.: Analysis of high streamflow extremes in climate change studies: how do we calibrate hydrological models?, Hydrology and Earth System Sciences, 26, 3863-3883, 10.5194/hess-26-3863-2022, 2022.

McMillan, H., Westerberg, I., and Branger, F.: Five guidelines for selecting hydrological signatures, Hydrological Processes, 31, 4757-4761, 10.1002/hyp.11300, 2017.

Moriasi, D. N., Arnold, J. G., Van Liew, M. W., Bingner, R. L., Harmel, R. D., and Veith, T. L.: Model evaluation guidelines for systematic quantification of accuracy in watershed simulations, Transactions of the Asabe, 50, 885-900, 10.13031/2013.23153, 2007.

Myneni, R., Knyazikhin, Y., and Park, T.: MOD15A2H MODIS/Terra Leaf Area Index/FPAR 8-Day L4 Global 500 m SIN Grid V006, NASA EOSDIS Land Processes DAAC [dataset], 10.5067/MODIS/MOD15A2H.006, 2015.

Nan, Y., Tian, F., Li, Z., and Gui, J.: Longer simulation time step of the tracer-aided hydrological model estimates lower contribution of slow runoff components, Journal of Hydrology, https://doi.org/10.1016/j.jhydrol.2023.129889, 2023.

Nan, Y., He, Z., Tian, F., Wei, Z., and Tian, L.: Can we use precipitation isotope outputs of isotopic general circulation models to improve hydrological modeling in large mountainous catchments on the Tibetan Plateau?, Hydrology and Earth System Sciences, 25, 6151-6172, 10.5194/hess-25-6151-2021, 2021a.

906 Nan, Y., He, Z., Tian, F., Wei, Z., and Tian, L.: Assessing the influence of water sampling
907 strategy on the performance of tracer-aided hydrological modeling in a mountainous basin
908 on the Tibetan Plateau, Hydrology and Earth System Sciences, 26, 4147-4167,
909 10.5194/hess-26-4147-2022, 2022.
910 Nan, Y., Tian, L., He, Z., Tian, F., and Shao, L.: The value of water isotope data on improving
911 process understanding in a glacierized catchment on the Tibetan Plateau, Hydrology and
912 Earth System Sciences, 25, 3653-3673, 10.5194/hess-25-3653-2021, 2021b.
913 Olsson, T., Jakkila, J., Veijalainen, N., Backman, L., Kaurola, J., and Vehvilainen, B.: Impacts
914 of climate change on temperature, precipitation and hydrology in Finland - studies using
915 bias corrected Regional Climate Model data, Hydrology and Earth System Sciences, 19,
916 3217-3238, 10.5194/hess-19-3217-2015, 2015.
917 Piani, C., Weedon, G. P., Best, M., Gomes, S. M., Viterbo, P., Hagemann, S., and Haerter, J. O.:
918 Statistical bias correction of global simulated daily precipitation and temperature for the
919 application of hydrological models, Journal of Hydrology, 395, 199-215,
920 10.1016/j.jhydrol.2010.10.024, 2010.
921 Rasouli, K., Pomeroy, J. W., and Marks, D. G.: Snowpack sensitivity to perturbed climate in a
922 cool mid-latitude mountain catchment, Hydrological Processes, 29, 3925-3940,
923 10.1002/hyp.10587, 2015.
924 Rasouli, K., Pomeroy, J. W., Janowicz, J. R., Carey, S. K., and Williams, T. J.: Hydrological
925 sensitivity of a northern mountain basin to climate change, Hydrological Processes, 28,
926 4191-4208, 10.1002/hyp.10244, 2014.
927 Reggiani, P., Hassanizadeh, S. M., Sivapalan, M., and Gray, W. G.: A unifying framework for
928 watershed thermodynamics: constitutive relationships, Advances in Water Resources, 23,
929 15-39, 10.1016/s0309-1708(99)00005-6, 1999.
930 Schaefli, B. and Gupta, H. V.: Do Nash values have value?, Hydrological Processes, 21, 99-
931 104, 2007.
932 Schaefli, B., Hingray, B., Niggli, M., and Musy, A.: A conceptual glacio-hydrological model
933 for high mountainous catchments, Hydrology and Earth System Sciences, 9, 95-109,
934 10.5194/hess-9-95-2005, 2005.
935 Stadnyk, T. A. and Holmes, T. L.: Large scale hydrologic and tracer aided modelling: A review,

936 Journal of Hydrology, 618, 10.1016/j.jhydrol.2023.129177, 2023.
937 Su, T., Miao, C. Y., Duan, Q. Y., Gou, J. J., Guo, X. Y., and Zhao, X.: Hydrological response to
938 climate change and human activities in the Three-River Source Region, Hydrology and
939 Earth System Sciences, 27, 1477-1492, 10.5194/hess-27-1477-2023, 2023.
940 Tang, Q. H., Lan, C., Su, F. G., Liu, X. C., Sun, H., Ding, J., Wang, L., Leng, G. Y., Zhang, Y.
941 Q., Sang, Y. F., Fang, H. Y., Zhang, S. F., Han, D. M., Liu, X. M., He, L., Xu, X. M., Tang,
942 Y., and Chen, D. L.: Streamflow change on the Qinghai-Tibet Plateau and its impacts,
943 Chinese Science Bulletin-Chinese, 64, 2807-2821, 10.1360/tb-2019-0141, 2019.
944 Tian, F., Hu, H., Lei, Z., and Sivapalan, M.: Extension of the Representative Elementary
945 Watershed approach for cold regions via explicit treatment of energy related processes,
946 Hydrology and Earth System Sciences, 10, 619-644, 10.5194/hess-10-619-2006, 2006.
947 Tian, F., Xu, R., Nan, Y., Li, K., and He, Z.: Quantification of runoff components in the Yarlung
948 Tsangpo River using a distributed hydrological model, Advances in Water Science, 31,
949 324-336, 2020.
950 Tong, R., Parajka, J., Salentinig, A., Pfeil, I., Komma, J., Szeles, B., Kuban, M., Valent, P.,
951 Vreugdenhil, M., Wagner, W., and Bloeschl, G.: The value of ASCAT soil moisture and
952 MODIS snow cover data for calibrating a conceptual hydrologic model, Hydrology and
953 Earth System Sciences, 25, 1389-1410, 10.5194/hess-25-1389-2021, 2021.
954 van Pelt, S. C., Kabat, P., ter Maat, H. W., van den Hurk, B., and Weerts, A. H.: Discharge
955 simulations performed with a hydrological model using bias corrected regional climate
956 model input, Hydrology and Earth System Sciences, 13, 2387-2397, 10.5194/hess-13-
957 2387-2009, 2009.
958 van Pelt, S. C., Kabat, P., ter Maat, H. W., van den Hurk, B. J. J. M., and Weerts, A. H.:
959 Discharge simulations performed with a hydrological model using bias corrected regional
960 climate model input, Hydrology and Earth System Sciences, 13, 2387-2397, 10.5194/hess-
961 13-2387-2009, 2009.
962 Wang, S., Liu, J., Pritchard, H. D., Ke, L., Qiao, X., Zhang, J., Xiao, W., and Zhou, Y.:
963 Characterizing 4 decades of accelerated glacial mass loss in the west Nyainqentanglha
964 Range of the Tibetan Plateau, Hydrology and Earth System Sciences, 27, 933-952,
965 10.5194/hess-27-933-2023, 2023.

966 Wang, T., Zhao, Y. T., Xu, C. Y., Ciais, P., Liu, D., Yang, H., Piao, S. L., and Yao, T. D.:
967 Atmospheric dynamic constraints on Tibetan Plateau freshwater under Paris climate
968 targets, Nature Climate Change, 11, 10.1038/s41558-020-00974-8, 2021.
969 Wang, Y. W., Wang, L., Zhou, J., Yao, T. D., Yang, W., Zhong, X. Y., Liu, R. S., Hu, Z. D., Luo,
970 L., Ye, Q. H., Chen, N. S., and Ding, H. T.: Vanishing Glaciers at Southeast Tibetan Plateau
971 Have Not Offset the Declining Runoff at Yarlung Zangbo, Geophysical Research Letters,
972 48, 10.1029/2021gl094651, 2021.
973 Wang, L., Han, S., Tian, F., Li, K., Li, Y., Tudaji, M., Cao, X., Nan, Y., Cui, T., Zheng, X., Hu,
974 Z., Wang, W., and Yang, Y.: The Evaporation on the Tibetan Plateau Stops Increasing in
975 the Recent Two Decades, Journal of Geophysical Research-Atmospheres, 127,
976 10.1029/2022jd037377, 2022.
977 Wang, L., Yao, T. D., Chai, C. H., Cuo, L., Su, F. G., Zhang, F., Yao, Z. J., Zhang, Y. S., Li, X.
978 P., Qi, J., Hu, Z. D., Liu, J. S., and Wang, Y. W.: TP-River: Monitoring and Quantifying
979 Total River Runoff from the Third Pole, Bulletin of the American Meteorological Society,
980 102, E948-E965, 10.1175/bams-d-20-0207.1, 2021.
981 Wu, Y., Long, D., Lall, U., Scanlon, B. R., Tian, F., Fu, X., Zhao, J., Zhang, J., Wang, H., and
982 Hu, C.: Reconstructed eight-century streamflow in the Tibetan Plateau reveals contrasting
983 regional variability and strong nonstationarity, Nature Communications, 13,
984 10.1038/s41467-022-34221-9, 2022.
985 Xu, R., Hu, H. C., Tian, F. Q., Li, C., and Khan, M. Y. A.: Projected climate change impacts on
986 future streamflow of the Yarlung Tsangpo-Brahmaputra River, Global and Planetary
987 Change, 175, 144-159, 10.1016/j.gloplacha.2019.01.012, 2019.
988 Xu, R., Tian, F., Yang, L., Hu, H., Lu, H., and Hou, A.: Ground validation of GPM IMERG and
989 TRMM 3B42V7 rainfall products over southern Tibetan Plateau based on a high-density
990 rain gauge network, Journal of Geophysical Research-Atmospheres, 122, 910-924,
991 10.1002/2016jd025418, 2017.
992 Yang, K. and He, J.: China meteorological forcing dataset (1979–2018), National Tibetan
993 Plateau Data Center [dataset], 10.11888/AtmosphericPhysics.tpe.249369.file, 2019.
994 Yao, T. D.: Tackling on environmental changes in Tibetan Plateau with focus on water,
995 ecosystem and adaptation, Science Bulletin, 64, 417-417, 10.1016/j.scib.2019.03.033,

2019.

Yao, Y. Y., Zheng, C. M., Andrews, C. B., Scanlon, B. R., Kuang, X. X., Zeng, Z. Z., Jeong, S. J., Lancia, M., Wu, Y. P., and Li, G. S.: Role of Groundwater in Sustaining Northern Himalayan Rivers, Geophysical Research Letters, 48, 10.1029/2020gl092354, 2021.

Yao, T. D., Bolch, T., Chen, D. L., Gao, J., Immerzeel, W., Piao, S., Su, F. G., Thompson, L., Wada, Y., Wang, L., Wang, T., Wu, G. J., Xu, B. Q., Yang, W., Zhang, G. Q., and Zhao, P.: The imbalance of the Asian water tower, Nature Reviews Earth & Environment, 3, 618-632, 10.1038/s43017-022-00299-4, 2022.

Yoshimura, K., Kanamitsu, M., Noone, D., and Oki, T.: Historical isotope simulation using Reanalysis atmospheric data, Journal of Geophysical Research-Atmospheres, 113, 10.1029/2008jd010074, 2008.

Zhang, T., Li, D., East, A. E., Walling, D. E., Lane, S., Overeem, I., Beylich, A. A., Koppes, M., and Lu, X.: Warming-driven erosion and sediment transport in cold regions, Nature Reviews Earth & Environment, 3, 832-851, 10.1038/s43017-022-00362-0, 2022a.

Zhang, T., Li, D. F., and Lu, X. X.: Response of runoff components to climate change in the source-region of the Yellow River on the Tibetan plateau, Hydrological Processes, 36, 10.1002/hyp.14633, 2022b.

Zhang, F., Zhang, H. B., Hagen, S. C., Ye, M., Wang, D. B., Gui, D. W., Zeng, C., Tian, L. D., and Liu, J. S.: Snow cover and runoff modelling in a high mountain catchment with scarce data: effects of temperature and precipitation parameters, Hydrological Processes, 29, 52-65, 10.1002/hyp.10125, 2015.

Zhao, Q., Ding, Y., Wang, J., Gao, H., Zhang, S., Zhao, C., Xu, J., Han, H., and Shangguan, D.: Projecting climate change impacts on hydrological processes on the Tibetan Plateau with model calibration against the glacier inventory data and observed streamflow, Journal of Hydrology, 573, 60-81, 10.1016/j.jhydrol.2019.03.043, 2019.